Oslo model, hyperuniformity, and the quenched Edwards-Wilkinson model

Peter Grassberger,[1] Deepak Dhar,[2] and P. K. Mohanty[3]
[1]*JSC, FZ Jülich, D-52425 Jülich, Germany*
[2]*Tata Institute for Fundamental Research, Mumbai, India*
[3]*Condensed Matter Physics Division, Saha Institute of Nuclear Physics, Kolkata, India*
(Received 8 June 2016; published 25 October 2016)

We present simulations of the one-dimensional Oslo rice pile model in which the critical height at each site is randomly reset after each toppling. We use the fact that the stationary state of this sand-pile model is hyperuniform to reach system of sizes $>10^7$. Most previous simulations were seriously flawed by important finite-size corrections. We find that all critical exponents have values consistent with simple rationals: $\nu = \frac{4}{3}$ for the correlation length exponent, $D = \frac{9}{4}$ for the fractal dimension of avalanche clusters, and $z = \frac{10}{7}$ for the dynamical exponent. In addition, we relate the hyperuniformity exponent to the correlation length exponent ν. Finally, we discuss the relationship with the quenched Edwards-Wilkinson model, where we find in particular that the local roughness exponent is $\alpha_{\rm loc} = 1$.

DOI: 10.1103/PhysRevE.94.042314

I. INTRODUCTION

Although self-organized critical (SOC) sand-pile models [1–6] have been studied intensively during the last 30 years, many of their aspects are still not well understood. For example, the critical exponents of avalanche distributions in the original Bak-Tang-Wiesenfeld (BTW) sand-pile model, on the square lattice, are still not known. The question of universality classes of different sand-pile models is also not well understood [7–9]. It is realized that models with stochastic toppling rules [10–16] have critical behavior different from those with deterministic toppling rules, and there may be more than one universality class corresponding to stochastic sand piles. In particular, models with stochastic toppling rules and with continuous local stresses (sand-pile heights) seem to have critical exponents significantly different from those with discrete ones [17]. On the other hand, as already noted by Tang and Bak [18–20], for all these models exist also non-self-organized versions, now called fixed-energy sand piles, that should show conventional (codimension one) critical points. The fixed-energy sand piles (FES) undergo an active-absorbing state transition as a function of the mean density of particles. An important question has been if this transition is in the universality class of directed percolation (DP). This question still remains somewhat controversial [10–16]. In FES, the number of absorbing states grows exponentially with the size of system. This alone would not create a problem, as it is known that models with many absorbing states can still be in the DP universality class, provided they do not have too-long-ranged correlations [21].

One problem in numerical studies is precisely the long-ranged correlations in the absorbing states at criticality, called in the following "natural critical states" (NCS). A straightforward strategy seems to consist in studying states remaining after large avalanches have died, in systems poised to the critical point. But, this is not possible since it is not feasible to wait until avalanches die on very large systems (the average CPU time per avalanche diverges with system size). Thus, one has to do some tricks that, unless one is sufficiently careful, can introduce spurious correlations in the NCS. While this problem was known quite early [22], it has been dealt with systematically only recently [15–17]. They indicated that there exists in fact a universality class of stochastic sand-pile models, but it seemed to be identical with the DP universality class. In fact, two of us have given heuristic arguments earlier, but no proof [15,16], that stochastic sand-pile models in the Manna universality class will flow into the DP universality class if we add an appropriate perturbation.

It is the purpose of this paper to clarify the situation somewhat. We study in detail the one-dimensional Oslo model [23,24], which is one of the simplest nontrivial stochastic sand-pile models. It has stochasticity in the toppling rules, and the critical height at each site is randomly reset after each toppling. Thus, it may be said that there is a degree of "stickiness" in the model. The model has some interesting properties due to its unusual algebraic structure. For example, for the boundary-driven model, it can be shown that if we start with the configuration with maximum height, just add one grain, and allow the system to relax, the distribution of probabilities of different stable final states reached is exactly the same as in the steady state. Also, the eigenvalues of the Markov matrix, which give the spectrum of relaxation times, is trivial with one eigenvalue 1, corresponding to the steady state, and all the rest are exactly zero [25]. However, the time-dependent correlation functions of the model are nontrivial because of the complication Jordan-block structure of the relaxation matrix.

We will study the behavior of other directed Oslo-type sand-pile models on the two-dimensional (2D) square lattice in a forthcoming paper. Here, we study the one-dimensional (1D) Oslo model using numerical simulations of much larger systems (and with much higher statistics) than what had been possible previously. As we said, simulations of FES *at the critical point* are hampered by the difficulty of sampling from the correct NCS. On the other hand, precise simulations of the SOC versions are difficult because the open boundary conditions lead to large finite-size corrections, unless one can simulate huge systems. The latter, however, is made difficult by very long transients (during which the proper NCS has to build up). As a consequence, the largest published simulations of the 1D Oslo model are for systems of size $\approx$20 000. Without the transients, systems larger by one or

two units of magnitude would be easy to simulate on modern computers.

Our large-scale simulations are made possible by two technical improvements: (i) we use a method of triggering avalanches in the FES that preserves all NCS correlations; (ii) we use initial configurations which are close to NCS configurations to reduce the time required to reach the NCS state.

Crucial for the latter is the observation, made first in [17] and verified later in [26–28], that NCS's of some SOC models are "hyperuniform" [29,30]. Consider a statistically stationary random point process on a line. Then, so long as correlations in the system die sufficiently fast with distance, using Gauss' central limit theorem, the variance of the number n_L of points in an interval of size L, $\mathrm{Var}[n_L] \sim L$. In contrast, a periodic distribution would have variance $\mathrm{Var}[n_L] \sim$ const. A point process on a line is called hyperuniform, if the variance falls between these two limits, more precisely,

$$\mathrm{Var}[n_L] \sim L^{\zeta} \tag{1}$$

with hyperuniformity exponent $0 < \zeta < 1$.

Notice that Eq. (1) implies negative long-range correlations, and it would be nontrivial to choose initial conditions which satisfy it exactly (with the correct exponent ζ), but this is not really needed. It will turn out that it is sufficient to use initial conditions which have (a) the right density, and (b) variances much smaller than those for random distributions. We shall use periodic initial conditions with long periods (typically $\gtrsim 10^2$) which are carefully chosen so that the density is close to the measured one of the NCS, the period is as small as possible for the given density, and the distribution within one period is as uniform as possible. We note that hyperuniformity is not a generic property of all sand-pile models. While the one-dimensional undirected sand-pile model does show hyperuniformity, the steady state of the prototypical BTW model on a square lattice, slowly driven by random particle additions, does not.

Our results can be summarized very succinctly: The 1D Oslo model is clearly not in the DP universality class. It is in the quenched Edwards-Wilkinson (qEW) class. This is consistent with the model studied in [15] being in the DP universality class, as all stochastic sand-pile models need not belong to the same universality class. Our estimates for the critical exponents $\nu = \frac{4}{3}$, $D = \frac{9}{4}$, $z = \frac{10}{7}$ are more precise than all previous estimates for any model in the Manna and/or qEW classes. They strongly indicate that *all* critical exponents are simple rationals. Finally, we have clear evidence that the SOC and FES versions of the 1D Oslo model are related to each other trivially, while this is still debated for the BTW model [31].

In the next section, we define the model and its variants, distinguished by boundary conditions and ways of driving. In Sec. III, we give some simulations details. In Sec. IV, we present the main numerical data for the determination of numerical exponents of the model. In Sec. V, we discuss the relationship to the quenched Edwards-Wilkinson model. Section VI contains a summary of our results, and some concluding remarks.

II. THE MODEL AND ITS VARIANTS

A. Driven at open boundary

The Oslo model was invented to mimic a one-dimensional pile of nonspherical particles (rice) [11]. In the original version, particles are added one after the other at the left end (which is closed), so that they pile up until they fall off from the open right end. Actually, as we shall see, it is more convenient to formulate it entirely in terms of local slopes, and to disregard completely the actual height of the pile. The reason is that we shall discuss later (in Sec. IV) a completely different interface associated with the local slopes, and we do not want to confuse the original height profile of the pile with it.

Because the slopes of the original pile will turn out to be *not* the slopes of the new interface, we will also change notation (even if this might be distracting at first) and speak of "stresses" instead of slopes.

Formally, the model is a one-dimensional cellular automaton where an integer $z_i \geqslant 0$ (the local stress) is attached to each site $i \in 1,2,\ldots,L$. Each site has a threshold stress z^*, which can be either 2 or 3; sites i with $z_i < z^*$ are called *stable*, whereas those with $z_i \geqslant z^*$ are unstable. Initially at $t = 0$, z^* at different sites are chosen (as 2 or 3) randomly and independently. Unstable sites immediately "topple" and reset their threshold values. For sites $1 < i < L$, toppling occurs as

$$z_i \to z_i - 2,\ z_{i\pm1} \to z_{i\pm1} + 1. \tag{2}$$

This corresponds to moving a single grain of rice from top of the pile at site i to site $i + 1$. At the boundaries, i.e., for $i = 1$ and L, only the appropriate neighbor gets increased, and the unit of stress that would go to $i = 0$ resp. $i = L + 1$ gets lost [32]. It is easily verified that in this stochastic model, topplings still have the Abelian property [4].

Using this property, it is possible to write a formal expression for the steady state of the model [33], both for the boundary- and bulk-driven cases. Unfortunately, these are not very useful for numerical studies, as the relaxation time required for a configuration with mean stress nearly equal to 2 is very long.

B. Boundary and bulk driving

In the original version, the model is driven by adding grains of rice at the left boundary. In terms of stresses, this means that the system is driven by increasing z_1 by one unit. If this leads to an instability, the entire avalanche of topplings is done before z_1 is increased again. A typical avalanche in the boundary-driven case, starting from a single seed, is shown in Fig. 1.

We say that the pile is bulk driven when we choose a random site $i \in]1,L[$ and increase its stress by 1 unit. Notice that this would be a somewhat unusual drive in a real rice pile: it would correspond to adding 1 rice grain at sites $1,2,\ldots,i$ each. We expect that avalanche size distributions for bulk driving will be different from those for the boundary-driven case, but some critical exponents like D and z (defined below) would be the same.

In addition, we expect that finite-size corrections will be very different. For boundary driving, the only large length scale is the distance L to the far boundary. For bulk driving, another length scale comes into play: the (random) distance of point of

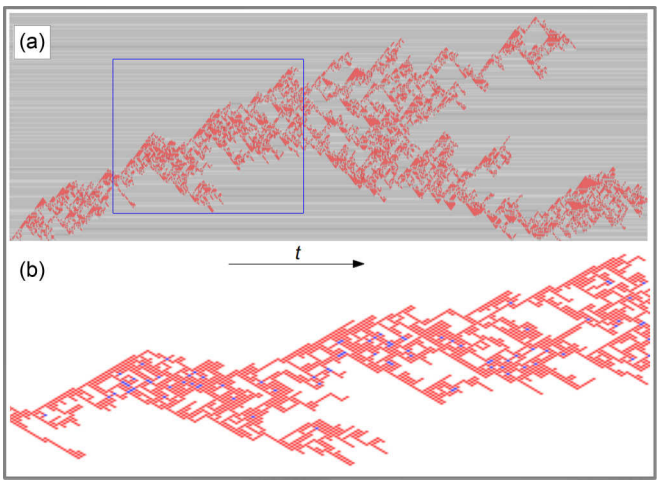

FIG. 1. A typical avalanche of boundary-driven Oslo model (time flows towards right). (a) The stress profile: $z_i \leqslant 2$ are marked as gray (different shades) and sites with $z_i > 2$ are marked as red. (b) A portion of the avalanche, marked as a rectangle in (a), is zoomed to view multiple topplings (marked differently).

addition from the boundary. This is, of course, averaged over, but typically gives rise to much larger finite-size corrections.

C. Fixed-energy version

Finally, we shall also consider the FES version with periodic boundary conditions. In that case, no stress can get lost. If we drive the system by adding stress, we sooner or later must reach the critical point where avalanches never stop. On the one hand, this is the cleanest case because finite-size corrections are minimal. On the other hand, as pointed out in the Introduction, simulations at the critical point are not trivial in this version.

In the subcritical case, simulations are rather straightforward: starting with any initial configuration with $\langle z\rangle = Z/L < z_c$, we follow the avalanche (if at least one site is unstable) until it dies. After that, all sites are stable. If $\langle z\rangle$ is sufficiently close to z_c, there will be some sites with $z_i = 2$. We now trigger a new avalanche by declaring one (or several) of these sites as unstable (if no site with $z_i = 2$ exists, we increase Z, until we are close enough to the critical point).

Note that, in our model, the critical thresholds at different sites in the steady state are independent random variables because they are randomly reset in the same way, independent of the history of the pile. Then, declaring a stable site with $z_i = 2$ unstable is equivalent to resetting the critical threshold at that site, and does not alter the NCS, hence, we do not expect to encounter the problems mentioned in [22].

Simulations are equally straightforward in the supercritical case, where the above procedure soon leads to an infinite avalanche. As in the BTW case [31], an avalanche will not stop after each site has toppled once, and this will happen in general after $\ll O(L)$ time steps.

On the other hand, following avalanches on large lattices until they die is not a viable option at the critical point because avalanches may not die even after very many time steps. In that case, we have (at least) three options as to how to proceed:

(a) We could use finite lattices and perform a finite-size scaling (FSS) analysis [34]. This gives reasonable results, although it requires more numerical effort and the extrapolation $L \to \infty$ is associated with the usual uncertainties of any extrapolation.

(b) We could introduce a small amount of dissipation [i.e., with some very small probability ϵ, Eq. (2) is modified such that one of the neighbors has its stress not increased], and extrapolate to $\epsilon \to 0$. This was the strategy used in [15,16]. While this should give cleanest results, it has the drawback that it requires more simulations and also involves an extrapolation. We did not try it in this work.

(c) We could simply cut the evolution at some large time $T_{\max}$. This seems to be the strategy chosen in most previous simulations (e.g., in the BTW simulations of [35]). As we shall see, results can be extremely misleading, unless this is done carefully.

D. Initial conditions

We know from previous simulations and from test runs that $z_c \approx 1.7326$. We now pick a rational number n/m slightly smaller than z_c, e.g., $n/m = 45/26 = 1.7307\ldots$. A sequence $w_{m,n}$ of m digits $z_i \in \{1,2\}$ is then constructed such that $\sum_i z_i = n$ and that $w_{m,n}$ is as uniform as possible. For $(n,m) = (45,26)$ such a sequence is $w_{26,45} = (12^2 12^3 12^3 12^3 12^2 12^3 12^3)$ or any of its cyclic permutations. The initial configuration is then simply a repetition of L/m such words, provided L is a multiple of m. In practice, we used rational approximants closer to z_c, such as 149/86 or 473/273.

E. Transients

First, we discuss transients in the boundary-driven case. To see most clearly the transients, we used very large lattices ($\geqslant 10^7$ sites) driven at the left boundary. We call the "active region" at time t the part $[1, i_{\max}(t)]$, where $i_{\max}(t)$ is the rightmost point that had toppled at some time $t' \leqslant t$. We monitor the evolution while $i_{\max}(t) < L$, i.e., while the active region still spreads. In Fig. 2, we show the total number of

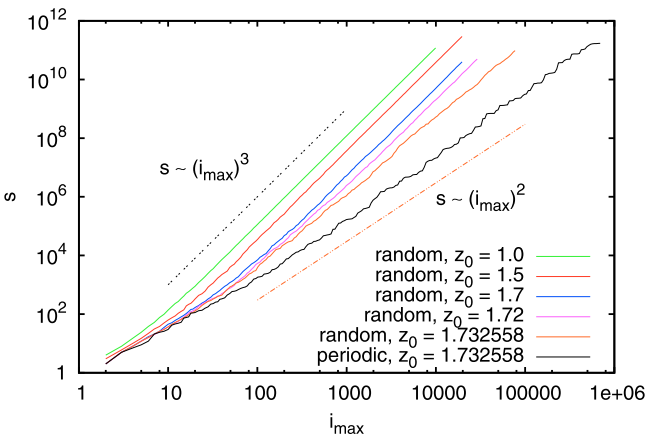

FIG. 2. Number of topplings on a semi-infinite lattice driven at its left end, until a site at distance $i_{\max}$ from this end is first toppled. Each curve is based on ≈1000 runs. The dashed red and black lines with slopes 2 and 3 are shown for comparison.

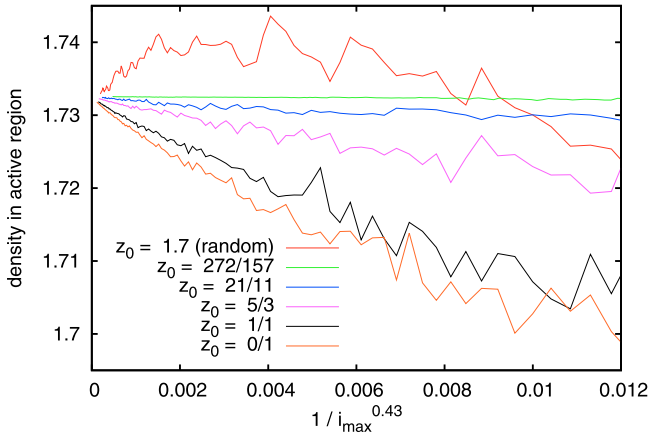

FIG. 3. Average density in the active region, plotted against an inverse power of the size $i_{\max}$ of the active region, for different initial configurations. Each curve is based on a single run. For all curves, the stationary density is reached as $i_{\max} \to \infty$, but the speed of convergence and the fluctuations depend strongly on the choice of initial state. Periodic initial states with density close to the stationary one are optimal. Notice that what looks like a horizontal straight line is indeed the data for $z_0 = 272/157 = 1.732\,484$.

topplings, starting from the initial time $t = 0$ until the time the disturbances from the boundary first reach the site $i = i_{\max}$, for different initial configurations. Notice that this gives a lower estimate for the transient CPU time because even if the active region covers the entire lattice, it is still not clear whether it has the correct NCS correlations. The top five curves are for random 1/2 sequences. If $z_0 = \langle z_{i,0}\rangle \ll z_c$, clearly $s \sim i_{\max}^3$. As z_0 comes closer to $z_c \approx 1.732\,60$, this increase is slower, but it is still much faster than the increase $s \sim i_{\max}^2$ observed for periodic initial configurations.

While Fig. 2 suggests that periodic initial configurations lead to much shorter transients, it could still be that the configurations at the time when $i_{\max}$ is reached have much larger fluctuations and densities far from the asymptotic one. That this is not true, and that periodic initial configurations lead both to much smaller fluctuations and to correct densities is seem from Fig. 3. There we plot the average density $\langle z\rangle_{\text{active}}$ in the active region, obtained in one single run, against an inverse power of $i_{\max}$. The lowest five curves in this plot correspond all to periodic initial configurations, with increasing values of z_0. They show that both deviations from the asymptotic density and fluctuations become smaller as the initial density approaches the stationary one. On the other hand, starting with a random configuration leads to huge fluctuations, even if its density is close to the stationary one.

III. DETERMINATION OF CRITICAL EXPONENTS FROM NUMERICAL SIMULATIONS

In Secs. III A to III C we shall mostly discuss simulations with open boundaries, which are driven by adding stress at the left boundary (with the exception of Figs. 2 to 6, which are indeed identical for open systems driven in the bulk). The fixed-energy version is discussed in Sec. III D, while properties of avalanches in bulk-driven open systems are treated in Sec. III E.

A. Stationary state and hyperuniformity

We will now discuss the various observables measured in our simulations, and their analysis in terms of the finite-size scaling theory. The critical exponent ν is defined in terms of the dependence of the correlation length ξ on the distance from the critical point $\epsilon = \rho - \rho^*$, where ρ^* is the critical density, by the relation

$$\xi \sim \epsilon^{-\nu}. \tag{3}$$

According to the finite-size scaling theory (FSS), a system with finite size L at criticality will behave like an infinite system with finite correlation length L. Thus, we expect

$$\langle z\rangle_L - z_c \sim L^{-1/\nu}. \tag{4}$$

The dependence of $\langle z\rangle_L$ on L provides a straightforward direct determination of ν. In Fig. 4, we show how the average stress $\langle z\rangle = L^{-1}\sum_{i=1}^{L} z_i$ depends on L. In the main plot we show the raw data, and in the inset a plot which suggests the precise finite-size corrections. Indeed, for reasons that will become clear in a moment, we used in Fig. 4 not only data obtained on boundary-driven systems, but we averaged also over systems driven in the bulk, both at random sites and also just at the center site. The result of Fig. 4 can be summarized as

$$\langle z\rangle = z_c + c/L^{\sigma} \tag{5}$$

with

$$z_c = 1.732\,594\,(4)\,, \quad \sigma = 1/\nu = \ 0.74(1), \tag{6}$$

while the precise value of c depends strongly on σ. The best previous estimates of z_c were 1.7326(3) for boundary-driven

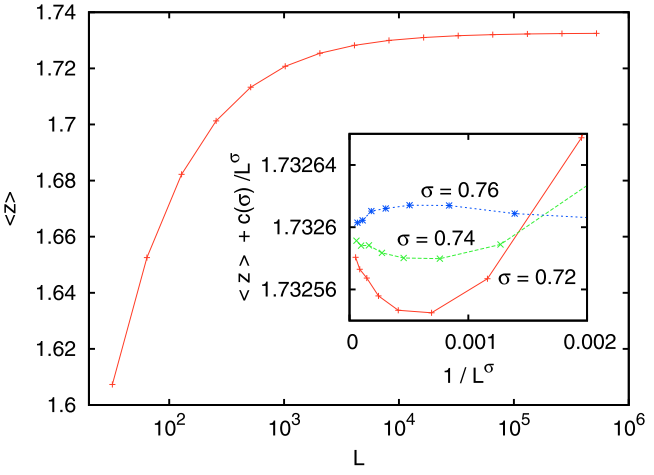

FIG. 4. Average stress $\langle z\rangle$ of driven systems with open boundaries as a function of L. Main: log-linear plot of the raw data. Inset: the same data plotted such that one can determine more precisely the finite-size corrections. More precisely, on the x axis is plotted $L^{-\sigma}$ with σ either 0.76, 0.74, or 0.72. If σ were equal to the exponent of the leading finite-size correction, then the plot of $\langle z\rangle$ versus $L^{-\sigma}$ would be asymptotically a straight line. Since finite-size corrections are very large, data would be indistinguishable from straight lines in such a plot for a wide range of σ. Therefore, we add to $\langle z\rangle$ a term linear in $L^{-\sigma}$, such that the curves become roughly flat near the origin. The curve which is most straight at the origin gives then the true correction to scaling exponent.

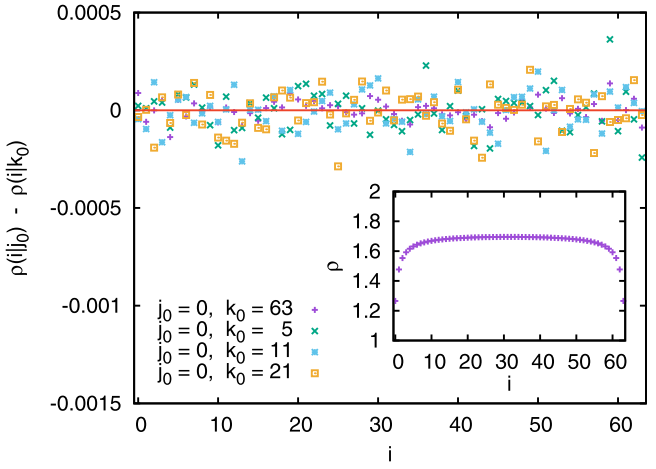

FIG. 5. The inset shows the stationary profile $\rho(i)$ for $L = 64$. To verify that it is indeed left-right symmetric, we show in the main plot differences between values of $\rho(i)$ measured at the same site i, but for runs where the system was driven at different values j_0 resp. k_0. The estimated statistical error for these differences was between ± 0.0001 and ± 0.0002.

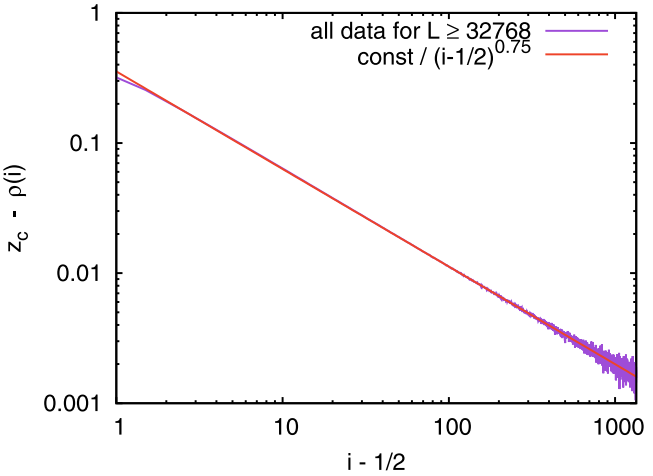

FIG. 6. Log-log plot of stress depletion near the end points versus distance from the end [more precisely from the point $x = \frac{1}{2}$, halfway between the site $i = 0$ where $\rho(i)$ is zero, and the site $i = 1$ where it first becomes positive]. Lattices ($L \geqslant 2^{15}$) are sufficiently large so that finite-size corrections should be negligible.

and 1.734(2) for bulk-driven open systems, and 1.732 60(2) for the FES version [34]. We are not aware of a previous estimate of σ.

Another way to determine ν is to look at the effects of the boundary on the density profile. Let $\rho(i)$ be the mean density of particles at site i in the steady state of the driven sand pile. From the Abelian property one obtains the following result: *$\rho(i)$ is independent of the way the pile is driven.*

Proof. Let a_i be the operator corresponding to adding a particle at i and letting a subsequent avalanche evolve until a stable state is reached again. Let $|\Phi\rangle$ be the statistically stationary (macro)state obtained by driving at site i with probability p_i. It satisfies $|\Phi\rangle = W|\Phi\rangle$ with $W = \sum_i p_i a_i$. Since all a_i commute due to the Abelian property, they can be diagonalized simultaneously, and $|\Phi\rangle$ is an eigenvector of each a_i with eigenvalue 1, and if the Markov process can reach all recurrent states, it is the only eigenvector with this property, and so independent of the distribution $\{p_i\}$.

We have checked this directly in simulations. In Fig. 5, we plot $\rho(i|j_0)$ the average stress at i when the system is driven at site j_0. In the main plot of Fig. 5 we show differences between averages measured at the same i but for different j_0. These data are for a very small system, but the same was found also for larger L. This is true also for random bulk driving, as we indeed verified numerically.

From scaling theory, we expect ρ_i to differ from z_c as

$$\rho(i) - z_c \sim i^{-1/\nu}. \tag{7}$$

We show the variation of ρ_i with i in Fig. 6.

The stress density, averaged over a finite block of size k, will in the critical state show fluctuations of order $k^{-1/\nu}$, hence the total stress Z in this block will fluctuate by a typical amount $k \times k^{-1/\nu}$. This gives

$$\mathrm{Var}[Z] \sim L^{\zeta} = L^{2(1-1/\nu)} \tag{8}$$

giving the hyperuniformity exponent $\zeta = 2(1 - 1/\nu)$. The variation of $\mathrm{Var}[Z]$ with k is plotted in Fig. 7. We see that the value of $\zeta = \frac{1}{2}$ fits the data very well. Based on the results presented, we conjecture that ν is exactly equal to the simple fraction $\frac{4}{3}$.

B. Avalanche size distributions

For the distribution of avalanches, our clearest data come from the boundary-driven case where one adds stress at the left boundary, and lets it dissipate through the right one.

Let us first discuss the avalanche size distribution $P(s,L)$, where s is the number of topplings in an avalanche. We expect the scaling law

$$P(s,L) = s^{-\tau} f[s/\varphi(L)] \times \left[1 + \frac{a}{s^x} + \ldots\right], \tag{9}$$

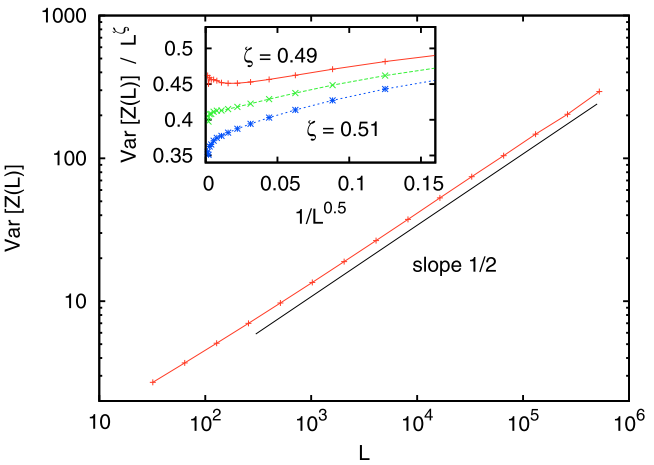

FIG. 7. The main plot shows a log-log plot of $\mathrm{Var}[Z]$ versus L, together with a straight line that suggests $\mathrm{Var}[Z] \sim L^{1/2}$ with visible corrections. The inset suggests that these corrections decrease roughly as $L^{-1/2}$.

with

$$\varphi(L) = L^D \times \left[1 + \frac{b}{L^\omega} + \ldots\right], \tag{10}$$

where the last factors in both expressions correspond to finite-size corrections.

In Fig. 8, we show $P(s,L)$ for values of L between 512 and 2^{18}. The raw data shown in panel Fig. 8(a) just demonstrate the impressive range, but they are not really informative. Multiplying the data with s^τ as in Fig. 8(b) shows already much more details. But, it still does not allow to make a precise estimate of τ. For this we have to include finite-size corrections, as in Fig. 8(c) [where we mostly plotted data for the smallest values of L, which were not shown in Figs. 8(a) and 8(b)]. The correction to scaling exponent is close to $\frac{1}{2}$, and we will justify the choice 0.4 below. Our best estimate of τ is 1.5556 ± 0.0005. This is a factor 4 more precise than the best previous estimates 1.556 ± 0.002 [24,37,38]. It strongly suggests that $\tau = \frac{14}{9}$ exactly, as conjectured in [39] (a 10 times more precise value was claimed in [39], but this was revised in a later paper by the same author [34]).

Using Eqs. (9), (10), and the fact that $\langle s\rangle = L$ (which is true exactly, without any finite-size corrections) gives

$$D = (2-\tau)^{-1} = 9/4 \pm 0.002 \quad \text{and} \quad \omega = xD \approx 0.9. \tag{11}$$

Superimposing the peaks in Fig. 8(b) would give a compatible but much less precise estimate of D because of the finite-size corrections in $\varphi(L)$. But a more precise value, with error bars similar as those that follow from the scaling relation, can be obtained from higher moments of s. From Eq. (9) we expect

$$\langle s^k\rangle \sim L^{(k+1-\tau)D} = L^{D+1} \times \left[1 + \frac{b'}{L^\omega}\right]. \tag{12}$$

In Fig. 9, we plot $L^{-y}\langle s^2\rangle$ against $1/L^{0.9}$ for three values of y. The central curve is for $y = \frac{13}{4}$, and it is a perfect straight line up to fluctuations for the two largest lattices ($L = 2^{18}$ and 2^{19}). On the other hand, the two other curves are clearly subcritical and supercritical. A similar result is obtained from the third moment (not shown). Apart from verifying the estimate of D, these data suggest very strongly that indeed the correction to scaling exponent is $\omega = 0.9$.

The distribution of spatial extensions of avalanches, $P_r(r,L)$, we assume the scaling form

$$P_r(r,L) \approx r^{-\tau_r} g(r/L), \tag{13}$$

As we have $s \sim R^D$, it is easily seen that $\tau_r = 1 + (\tau - 1)D$. For $D = \frac{9}{4}$ and $\tau = \frac{14}{9}$, we get $\tau_r = \frac{9}{4}$.

Plots analogous to Figs. 8(b) and 8(c) are shown in Fig. 10. This time the corrections to scaling are much bigger, but they seem to be described again to leading order by a rational power. The value $\tau_r = \frac{9}{4}$ fits our data well, with an error of ± 0.002. At the same time, accepting the scaling $s \sim r^D$ in the scaling region, we predict the correction to scaling exponent as $0.4 \times \frac{9}{4} = 0.9$, in perfect agreement with the data.

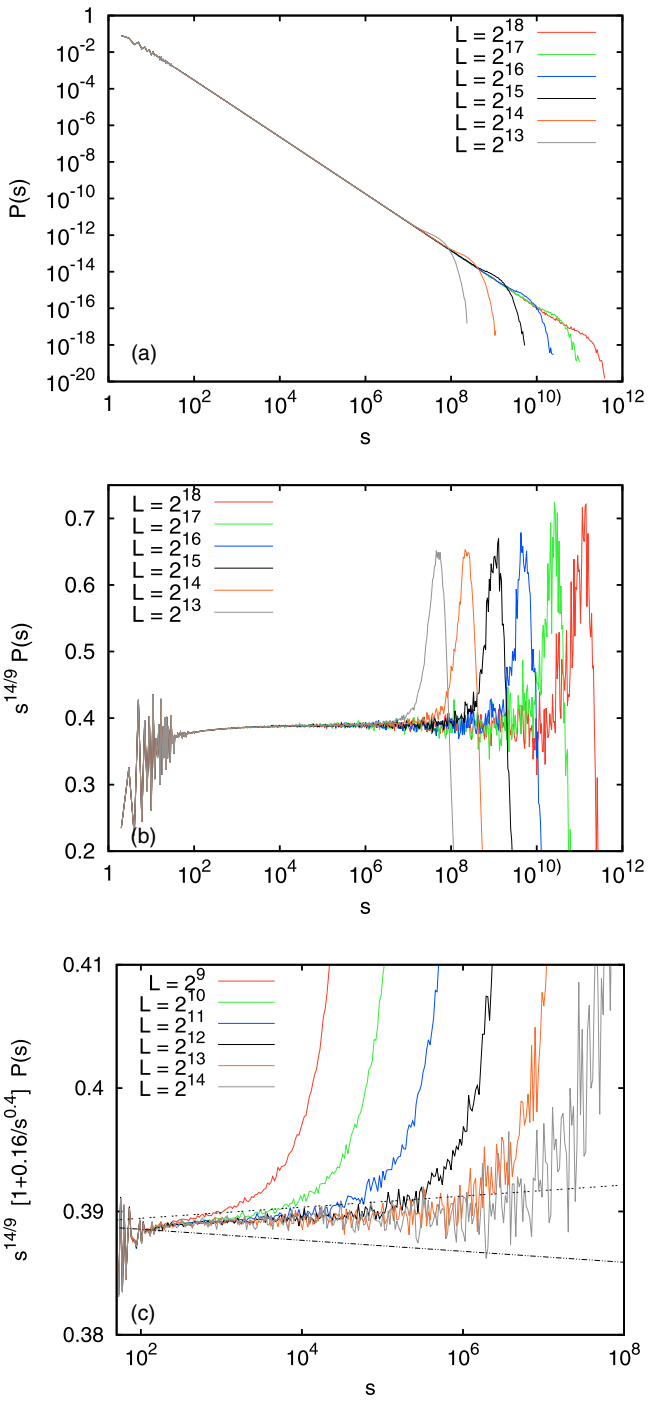

FIG. 8. Avalanche size distributions for the open systems driven at the left boundary. (a) Shows the raw data (for the largest lattices sizes only, to avoid overcrowding). (b) Shows the same data multiplied by $s^{14/9}$. If this exponent is equal to τ, the central parts of the curves should be flat. In view of the substantial corrections to this, we plotted in (c) the data (for smaller L, since they have less statistical fluctuations) multiplied by a further factor $(1 + a/s^x)$, with $x = 0.4$. The two straight lines in (c) indicate the error margins ± 0.0005 of τ. The numbers of avalanches used for these figures range between $>2 \times 10^{10}$ for $L \leqslant 4096$, 1.7×10^9 for $L = 131\,072$, and 3.5×10^9 for $L = 262\,144$. The fluctuations seen for $s < 100$ are not statistical, but are systematic, and are related to the structure of the state-space of recurrent stable configurations [36].

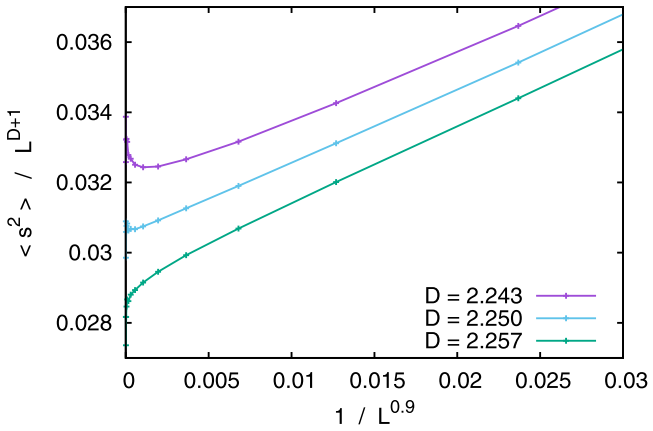

FIG. 9. Rescaled second moments of avalanche sizes for the boundary model, plotted against $1/L^{0.9}$. The moments are divided by powers of L, such that the curve would be straight if the power were equal to $D+1$ and the correction to scaling exponent were $\omega = 0.9$. This is indeed the case for $D = \frac{9}{4}$. The other two curves (with exponents $\frac{9}{4} \pm 0.007$) are clearly subcritical and supercritical.

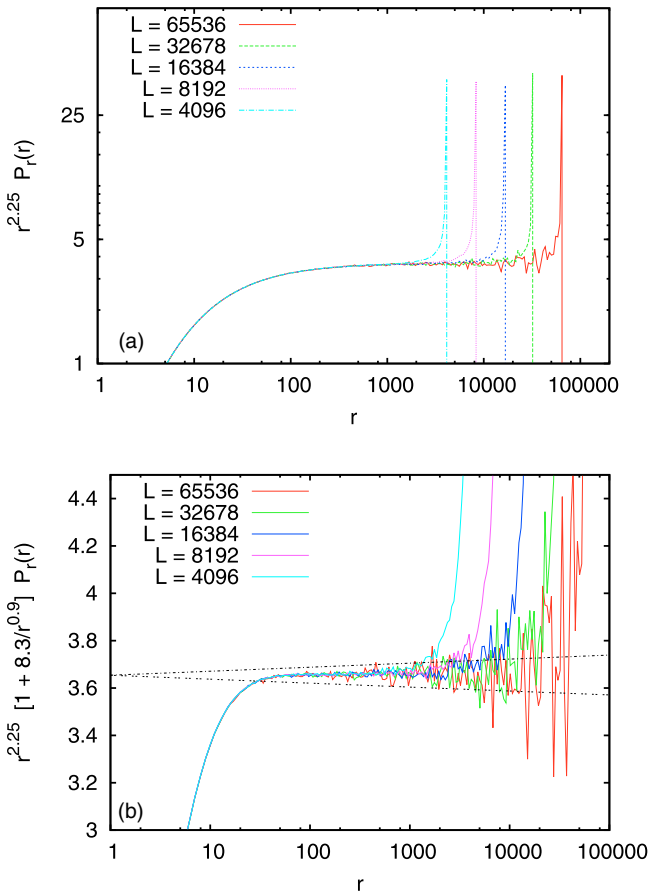

FIG. 10. (a) Log-log plot of $P_r(r,L)$, the spatial size distribution of avalanches for boundary-driven systems, multiplied by $r^{9/4}$. (b) The same data, but multiplied by $1 + 8.3/r^{0.9}$ and plotted on a log-linear plot. The straight lines indicate the estimated errors ± 0.002.

C. Temporal evolution of avalanches

We now discuss the time-dependent exponents of the avalanches. We define the dynamical exponent z by the relation

$$R(t) \sim t^{1/z}, \tag{14}$$

where $R(t)$ is the average distance of topplings at time t from the boundary where the avalanches were triggered. Other related quantities are $P_t(t)$ and $N(t)$, which are, respectively, the probability that the avalanche survives up to time t, and the average number of topplings at time t in the avalanches that survive up to time t. We define the exponents η and δ by the relations

$$P_t(t) \sim t^{-\delta} \quad \text{and} \quad N(t) \sim t^{\eta}. \tag{15}$$

Results of these measurements are shown in Fig. 11. They all show very clean scaling regions, with

$$\delta = 7/8, \quad \eta = -3/10, \quad \text{and} \quad z = 10/7. \tag{16}$$

We do not quote formal error bars because by now we obviously conjecture that these rational numbers are exact, and any error estimate (which by its very nature is subjective, critical exponents being obtained by *extrapolating* data) would probably be biased by this conjecture. We nevertheless can say informally that plots analogous to Figs. 8(c) and 10(b) suggest $\delta = 0.875(1)$, $\eta = -0.300(1)$, and $1/z = 0.700(2)$.

Typical previous estimates were $\delta = 0.85(2)$, $\eta = 0.33(2)$, and $z = 1.42(2)$ [40]. They were, however, made by assuming a Manna universality class and thus lumping together simulation results from various models. As a rule of thumb, our present estimates are an order of magnitude more precise than previous ones. On the other hand, extracting correction to scaling exponents from Fig. 11 was not very successful because obviously more than one correction term is important in each case. Presumably, there are also important analytic corrections resulting from an inherent uncertainty how to define t up to an arbitrary constant of order 1.

Another estimate of z can be obtained from the moments of T, the lifetime of avalanches. When defining $\langle T^k \rangle$, one has to specify how avalanches with different size s are weighted. In Fig. 12, we show results where $T = s^{-1} \sum_{\text{topplings } j} t_j$ and t_j is the time of the jth toppling in the parallel update scheme. To make the plot more significant, we do not plot the raw data, but rather divide them by the expected power laws

$$\langle T^k \rangle \sim L^{b_k} \tag{17}$$

with $b_k = (\delta + k - 1)z$. Obviously, the data are compatible with this prediction. The clearest agreement holds for $k = 2$. For $k = 1$ we see very large finite-size corrections, while individual outliers cause large statistical fluctuations for $k = 3$. Nevertheless, the data shown in Fig. 12 fully support our previous estimates of δ and z.

D. Fixed-energy sand pile: Closed boundaries case

1. *Supercritical systems: The order parameter exponent*

As we said in the Introduction, simulating the fixed "energy" (i.e., stress) model is easiest and most straightforward away from the critical point. In contrast, measuring the properties of single avalanches is nontrivial both in the critical

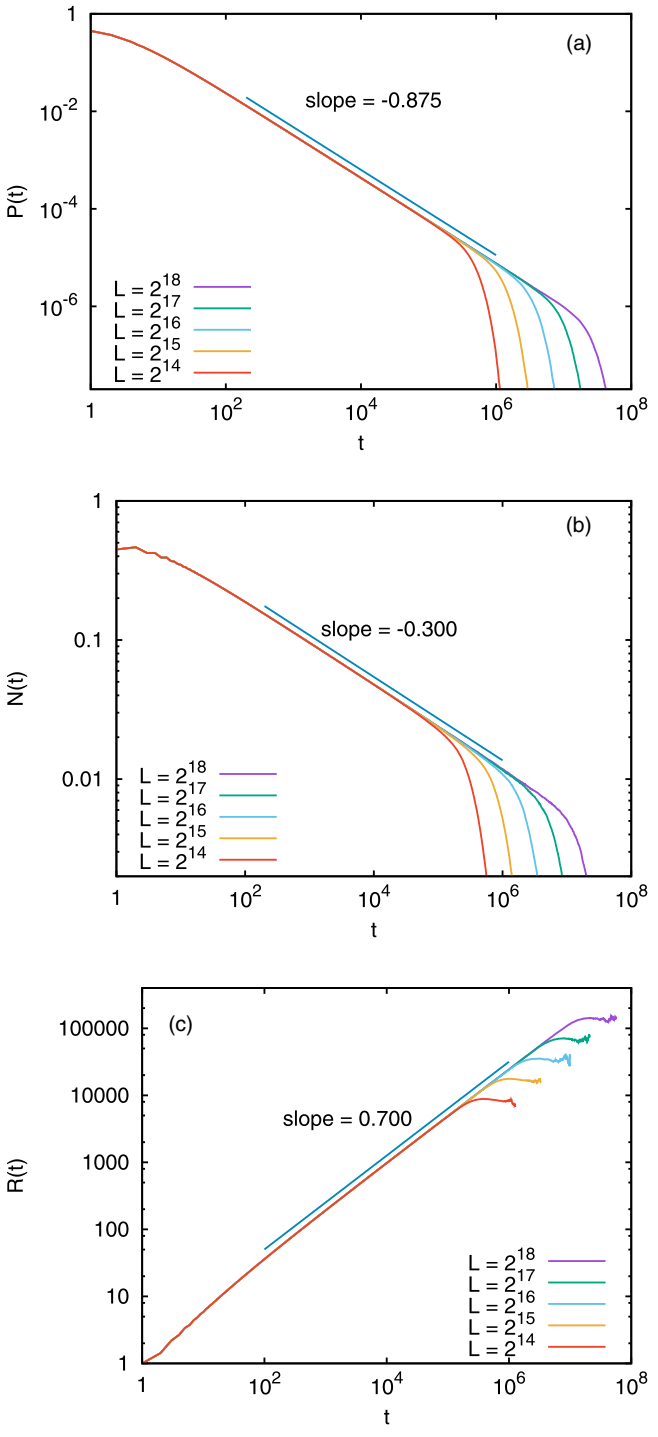

FIG. 11. Log-log plot of $P_t(t,L)$ (a), $N(t,L)$ (b), and $R(t,L)$ (c). In each plot, only data for $L \geqslant 16\,384$ are shown. The straight lines indicate power laws in the central (scaling) region.

and in the supercritical phase. But, estimating the density $\rho_{a,\infty}$ of active sites in a stationary supercritical state, and thus the order parameter β defined through

$$\rho_{a,\infty} \equiv \lim_{t\to\infty} \rho_a(t) \sim (\langle z\rangle - z_c)^{\beta}, \tag{18}$$

is easy. We start with a periodic configuration with the desired total stress (which implies also that we use for L a multiple of the period). There will be $O(L)$ sites with $z_i = 2$, half of which

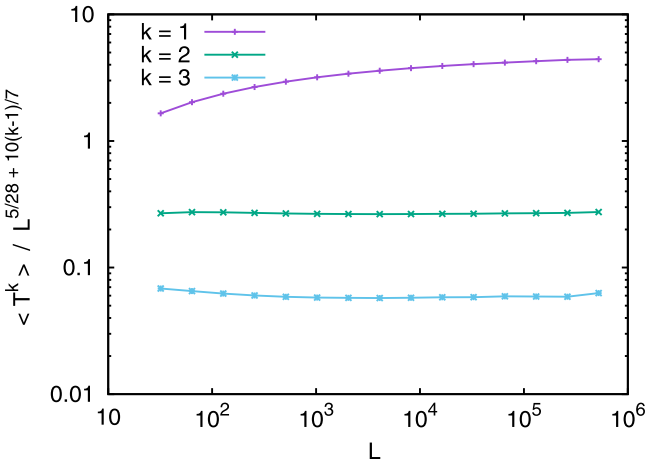

FIG. 12. Log-log plots of rescaled lifetime moments $\langle T^k\rangle/L^{(\delta+k-1)z}$ of boundary-driven avalanches, with $k = 1$, 2, and 3. Apart from finite-size corrections and statistical fluctuations, the data are supposed to fall on straight horizontal lines.

are declared as unstable. We then follow the evolution until stationarity of ρ_a is reached and enough statistics is collected thereafter.

The approach to stationarity will be roughly exponential in the far supercritical regime, but in the critical region it will follow a power law. In the latter region, the difference between the periodic initial state and the true NCS will become important, and we shall defer the discussion of this subtle case to a later subsection. Here, it is sufficient to point out that in the worst case (i.e., closest to the critical point, where the correlation length becomes comparable to L) the transient time increases as L^z. As we have seen, the correlation length scales as $\xi \sim (\langle z\rangle - z_c)^{-\nu}$ with $\nu = \frac{4}{3}$. Thus, we can use lattices of sizes up to $L \approx 10^6$, simulated over $5\times \approx 10^7$ time steps, to test Eq. (18) down to $\langle z\rangle - z_c \approx 0.000\,05$.

Figure 13 shows results from such runs. Each point in this plot is obtained from at least 40 such runs, and it was verified

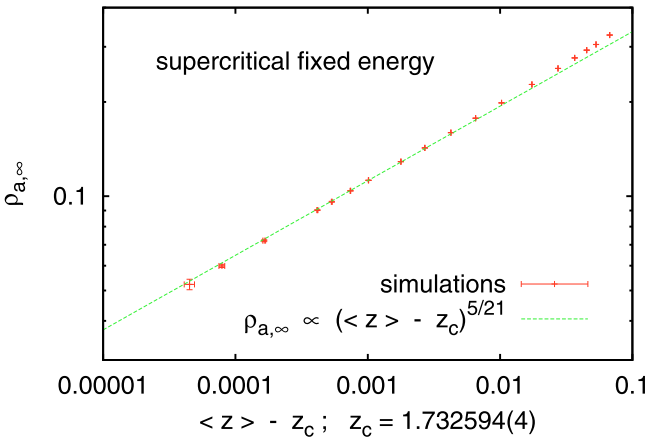

FIG. 13. Log-log plot of $\rho_{a,\infty}$ against $\langle z\rangle - z_c$. The straight line indicates the power law predicted by the scaling theory. The best fit would indeed be obtained with an exponent 0.243(5). The leftmost point was obtained by simulating 40 lattices with $L = 10^6$ for 5×10^7 time steps.

that the density of activity had become stationary. The straight line indicates the exponent

$$\beta = 5/21 \tag{19}$$

that follows from the scaling theory discussed below. The data shown in the figure would by themselves give a best fit $\beta = 0.243(5)$, compatible with the above.

To obtain Eq. (19), we notice first that FSS implies that for finite L and exactly at criticality $\rho_{a,L} \sim L^{-\beta/\nu}$. The number of topplings in large avalanches (those which dominate the higher moments of s) scales then as L times this density times the duration of the avalanches

$$s \sim L \times L^{-\beta/\nu} \times L^{z}. \tag{20}$$

Assuming that $s \sim L^{D}$ with $D = \frac{9}{4}$ gives then

$$\beta = (1 + z - D)\nu = 5/21. \tag{21}$$

There exist a large number of previous estimates of β, either for the Oslo model itself or for other models which are supposed in the same (Manna) universality class (see Table I). They are all are much bigger, with one notable exception: $\beta = 0.24(3)$ was obtained in [40]. All other estimates are supposedly more precise but outside our error bars. The problem in determining β is obviously the large corrections to scaling which are seen in Fig. 13, and which require very large systems to be studied. In Table I we quote also the value for DP. In many previous papers it was concluded that the Manna class has to be distinct from DP, mainly because it has a *larger* value of β. We see now that the opposite is true, and Oslo $\neq$ DP because its β is *smaller* than that of DP.

We include in Table I also three estimates for the qEW model. Since the mapping of the Oslo model onto interface pinning is such that the interface height is just the number of topplings, the activity density $\rho_a(t)$ is just the average speed of the interface at time t. The value quoted in Table I is for the exponent (called θ in [51,52]) that described how the speed increases in the depinned phase with the distance from the critical point $v \sim (F - F_c)^{\theta}$.

In [53], the relation between

$$\beta = (1 + z - D)/(3 - D) \tag{22}$$

was proposed. Although the numerical value of β obtained thereby in [53] is different from ours, Eq. (22) is satisfied by our exponents. Together with Eq. (19) it gives

$$\nu = 1/(3 - D). \tag{23}$$

Finally, we note that for FES with deterministic toppling rules, it has been noted that the critical density at which infinite avalanches first appear, depends on the starting configuration [31]. For sand piles with stochastic toppling rules, this is not a problem, and the SOC and FES versions of the Oslo model have the same critical density.

TABLE I. Estimates of the critical exponent β defined in Eq. (18). The acronyms for the various models are explained in the references.

0.24(3)	[40]	Overall Manna class
0.42(2)	[41]	Manna
0.416(4)	[42]	Restricted Manna
0.41(1)	[43]	Restricted Manna
0.289(12)	[44]	Restricted Manna
0.29(2)	[45]	CDP
0.28(2)	[46]	CDP
0.382(19)	[47]	DCMM
0.277(18)	[17]	CCMM
0.308(2)	[17]	CTTP
0.275(6)	[17]	CLG
0.277(3)	[48]	Modified CLG
0.25(3)	[49]	qEW
0.33(2)	[50]	qEW
0.250(3)	[51,52][a]	qEW
0.245(6)	[54]	qEW
0.396(5)	[55]	Oslo
0.243(5)	This work	Oslo, direct fit
$5/21 = 0.2380\ldots$	This work	Oslo, scaling relation
$0.2764\ldots$	[21]	DP

[a]A more precise value was given in [51]; the value cited here is the one given later in [52].

2. *Subcritical single-seed avalanches*

The next easy case involves isolated avalanches in the subcritical phase. We again start with a periodic configuration (this time with $\langle z \rangle < z_c$). We declare all sites (including those with $z_i = 2$) as stable. To trigger an avalanche, we simply pick a random site among those with $z_i = 2$ and declare it as unstable. This avalanche will be finite with probability 1 and will have also finite size, thus, we can follow its evolution until it dies and the configuration is stable again. After that, we again declare a random site with $z_i = 2$ as unstable and repeat.

By measuring avalanche sizes, we verified that transients are very short: average avalanche sizes converge within error bars to a stationary value, after each site has toppled less than 1000 times, even when $\langle z \rangle$ is very close to z_c. Thus, we can again get good statistics for lattices with L up to 10^6. Lattices of this size are indeed needed in order to avoid finite-size effects, if we want to measure very close to the critical point.

Results are shown in Fig. 14, where we plot $\langle s \rangle$ against the distance from the critical point. We see a clear power law in the critical region, but important scaling corrections when $z_c - \langle z \rangle$ becomes large. The latter could have suggested that the power is the same as for DP, but this is actually excluded: While the DP exponent γ, defined as

$$\langle s \rangle \sim (z_c - \langle z \rangle)^{-\gamma}, \tag{24}$$

is 2.278 [21], a direct fit to our data would give $\gamma = 2.68(2)$. The upper straight line shown in Fig. 14 represents our scaling conjecture

$$\gamma = 2\nu = \ \ 8/3, \tag{25}$$

which follows from $\langle s \rangle \sim L^2$ via FSS and which is fully compatible with the directly measured value.

3. *Finite-size scaling: Critical avalanches on finite lattices*

Exactly at the critical point, we cannot use either of the two strategies discussed in the previous subsections. In this section we simulate single avalanches, triggered in the way described above, on lattices of sufficiently small L so that we can follow all of them until they die. Avalanche distributions

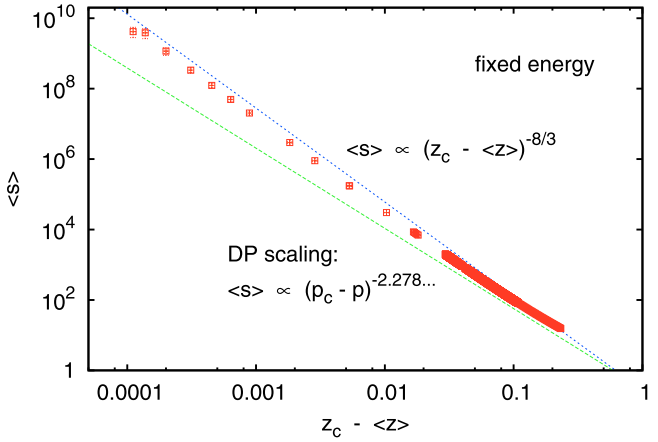

FIG. 14. Log-log plot of $\langle s\rangle$ against $z_c - \langle z\rangle$ for subcritical avalanches in the FES version. The upper straight line indicates the power law predicted by the scaling theory. The best fit would indeed be obtained with an exponent 2.68(2). The lower straight line shows the behavior that would have been expected, if the Oslo model were in the DP universality class. The leftmost point was obtained by simulating 3600 avalanches on a lattice with $L = 5 \times 10^5$.

will be discussed below, but first we shall discuss moments of their sizes and durations.

Moments of the avalanche size s are shown in Fig. 15(a), while moments of their lifetimes are shown in Fig. 15(b). The latter were computed as in Sec. III C. In Fig. 15(a) we show results for three values of $\langle z\rangle$ close to z_c, while results for only two of them are shown in Fig. 15(b).

The bottom triple of curves in Fig. 15(a) show $\langle s\rangle/L^2$. These values are independent of L within errors for the central curve which is essentially critical, showing that

$$\langle s\rangle \sim L^2 \tag{26}$$

for critical avalanches in the FES ensemble, just as it is for bulk-driven avalanches on open lattices. This is not entirely trivial since the argument predicting this scaling for open systems no longer holds. The fact that we nevertheless find the same scaling in both ensembles is a strong indication that the avalanches have the same statistical properties.

The same conclusion is reached by looking at the two upper triples of curves in Fig. 15(a) which show the ratios $L^{-2}\langle s^k\rangle/\langle s^{k-1}\rangle$ for $k = 2$ and 3. Here, the critical curves show that all moments satisfy exactly the same critical scaling $\langle s^{k+1}\rangle \sim L^{2+9k/4}$ as for open systems.

The data for avalanche durations shown in Fig. 15(b) tell a similar story. The two topmost pairs of curves show that $\langle T^k\rangle/\langle T^{k-1}\rangle$ with $k \geqslant 2$ scale with the same power of L, which is within errors the same as the exponent z found also in the open case [the fitted value of z now is 1.438(10), while our previous estimate was $10/7 = 1.4286$]. In agreement with the bulk-driven open case, $\langle T\rangle$ now also shows good scaling, with exponent 1.187(10).

Distributions of avalanche sizes and of the three time-dependent properties $P_t(t)$, $N(t)$, and $R(t)$ are shown in Fig. 16 we did these simulations at $\langle z\rangle = 1.732\,601$ before arriving at the final estimate for z_c in Eq. (6), but the small deviation from the best estimate of z_c should not matter much. For $P(s)$ we

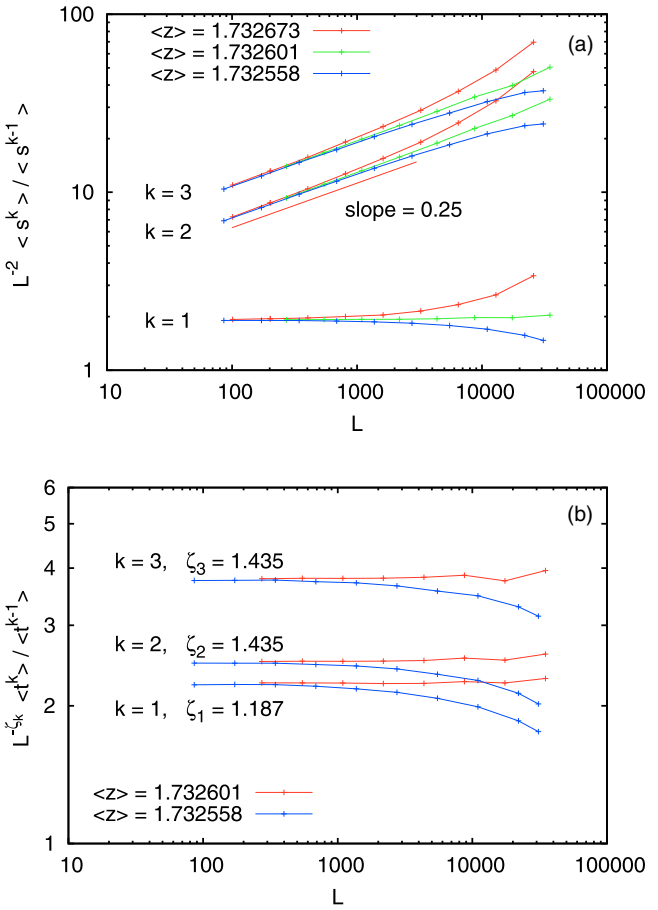

FIG. 15. (a) Log-log plot of $\langle s\rangle$ (lowest triple of curves) and $\langle s^k\rangle/\langle s^{k-1}\rangle$ for $k = 2$ and 3 (topmost triples) against L. Each curve in each triple corresponds to a different periodic start configuration (periods 101, 273, and 86 from top to bottom), and each value of L is a multiple of the corresponding period. The data are divided by L^2 which makes the central curve in the lowest triple horizontal and makes the central curves in the two upper triples scale as $L^{1/4}$ (straight line). (b) Analogous results size weighted for moments of avalanche lifetimes. This time only data for the two smaller values of $\langle z\rangle$ are shown, and all data are divided by powers of L which make the critical curve of each pair horizontal.

show only a plot analogous to Figs. 8(b) and 23, where we divided the raw data by the supposed power law $s^{-\tau_{\rm bulk}}$ (see Fig. 17). Although the scaling is not perfect, the improvement compared to the bulk-driven case with open boundaries shown in Fig. 23 is dramatic. Now, we can argue rather convincingly that $\tau_{\rm bulk} = \frac{10}{9}$. The best estimate based on this plot alone would be $\tau_{\rm bulk} = 1.10(1)$, based both on the scaling region and on the heights of the peaks (which should also scale as $s^{-\tau_{\rm bulk}}$).

The three panels of Fig. 16 show $t^{7/40}P_t(t)$, $t^{-2/5}N(t)$, and $t^{7/10}R(t)$. The actual best exponent estimates based on these plots alone would be $\delta_{\rm bulk} = 0.175(3)$, $\eta_{\rm bulk} = 0.398(3)$, and $z_{\rm bulk} = 0.699(3)$, as indicated by the dashed straight lines in each panel.

Within the statistical errors, the sum $\delta + \eta$ is the same as for open boundary-driven systems:

$$\delta_{\rm bulk} + \eta_{\rm bulk} = \delta + \eta = 23/40. \tag{27}$$

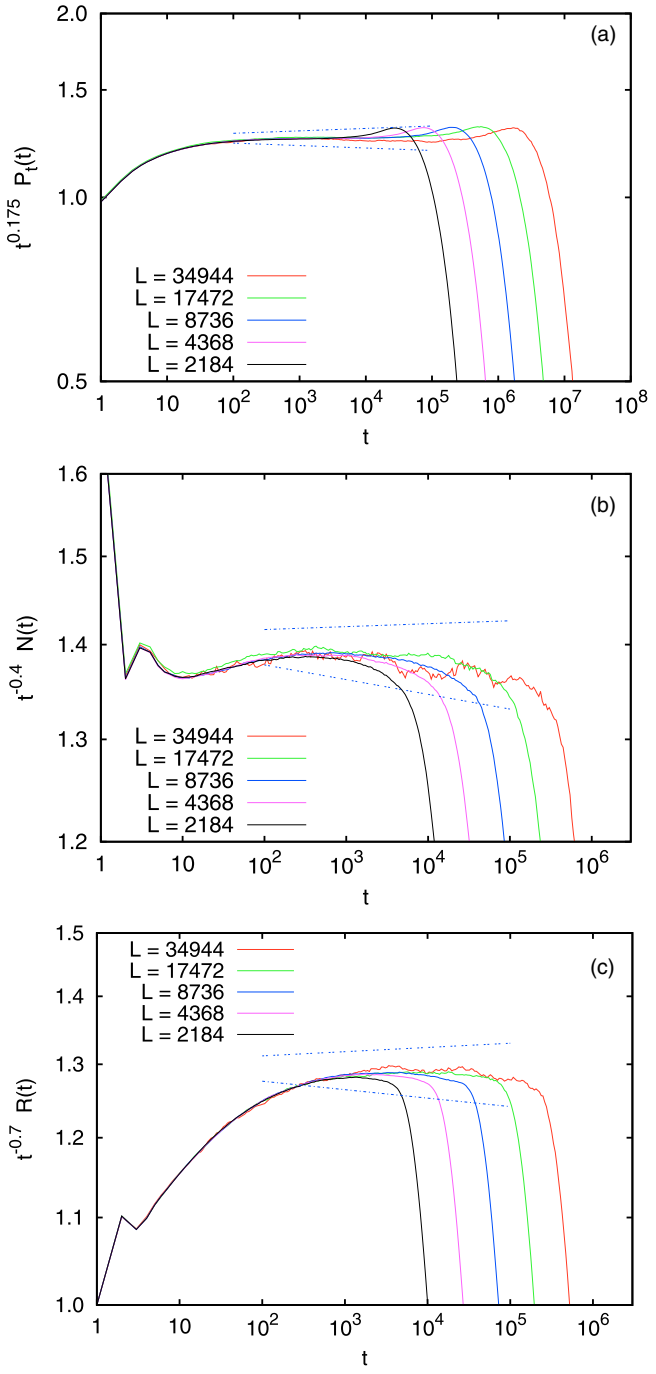

FIG. 16. Log-log plots of $P_t(t,L)$ (a), $N(t,L)$ (b), and $R(t,L)$ (c). In each plot, the raw data were divided by the conjectured power laws, i.e., the actually plotted data are $t^{7/40}P_t(t,L)$, $t^{-2/5}N(t)$, and $t^{-7/10}R(t)$. As in Fig. 17, $R(t)$ is the rms distance from the first toppling. In each panel, the straight lines indicate the error bars mentioned in the text.

This means that the activity $N(t)/P_t(t)$ per *surviving* avalanche shows the same scaling in both cases. It should indeed scale as the product of the activity density in the active region (which scales as $t^{-\beta/z/\nu}$, as we shall see later) times its spatial extent (which scales as $t^{1/z}$). Therefore,

$$\delta + \eta = (1 - \beta/\nu)/z. \tag{28}$$

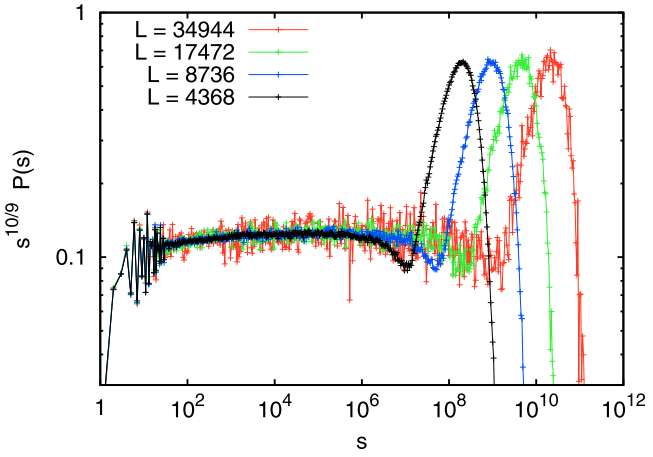

FIG. 17. Log-log plot of the avalanche size distributions for the fixed-energy version at $\langle z\rangle = 1.732\,601$, and for different lattice sizes which are all multiples of 273. The actually plotted data are $s^{10/9}P(s)$.

4. Simulations involving termination of the evolution in nonstationary states

So far, we have only discussed simulations of the fixed-energy Oslo model where it was either not necessary to terminate the evolution because avalanches died anyhow, or where the system had already reached a stationary state. For simulating systems very close to the critical point, it seems, however, necessary to terminate the evolution before avalanched have died or before stationarity is reached. As we shall see, extreme case is needed in interpreting such simulations.

Let us first discuss simulations of single avalanches, triggered by declaring random sites with $z_i = 2$ in an otherwise stable configuration as unstable. If an avalanche survives for a time $>t_{\max}$, its evolution is cut off by declaring all sites with $z_i = 2$ as stable. Since only very few avalanches survive until $t_{\max} \gg 1$, one might hope that this gives reasonable results if $t_{\max}$ is sufficiently large. Indeed, this strategy is rather common in studies of FES sand-pile models. Figure 18 shows survival probabilities $P_t(t)$ on very large lattices and at $\langle z\rangle$ very close to criticality, for different values of the cutoff $t_{\max}$, ranging from 10^4 to 2×10^7. Since we have multiplied the data by the factor t^δ, we should have expected the curves to become horizontal for large t and large $t_{\max}$. They do indeed become horizontal for $1 \ll t \ll t_{\max}$, but estimating δ from the data with largest t would give gross inconsistencies. The same is true for $N(t)$, $R(t)$, and $P(s)$. In all these cases we could get consistent results by first taking $t_{\max}\to\infty$ and only then going to large t, but this would not be very practical.

The reason for this failure is that if avalanche evolution is stopped at $t_{\max}$, also the correlations in the NCS needed to make it critical and hyperuniform cannot develop at distances $>t_{\max}^{1/z}$. Essentially, criticality and hyperuniformity are then confined to scales $<t_{\max}^{1/z}$ and correlations at larger scales are those of the initial state and different from those in the NCS, even if the simulation is kept going for extremely long times (see Fig. 19). Since total CPU time was roughly the same for each curve in Fig. 19, it seems unlikely that longer runs would establish critical correlations on substantially larger scales.

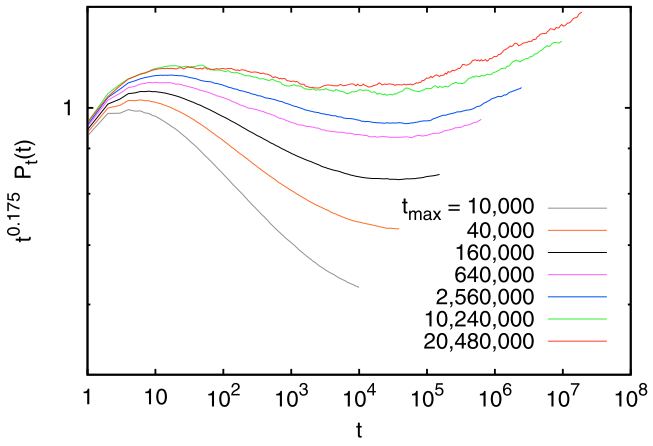

FIG. 18. Log-log plots of rescaled survival probabilities $t^{7/40}P_t(t)$, if the evolution of each still surviving avalanche is terminated at time t_{max}. Here, the largest lattices (for the largest t_{max}) had $L = 2^{21}$. The average stress was 1.732 591 (i.e., slightly subcritical), but it was verified that results were indistinguishable at slightly supercritical $\langle z\rangle$. From our previous simulations we would have expected the curves to become horizontal for large t and large t_{max}.

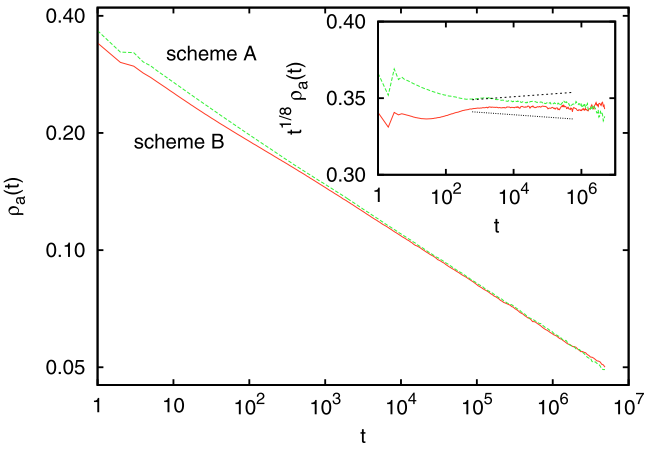

FIG. 20. Main plot: log-log plot of $\rho_a(t)$ for $\langle z\rangle = 359/208 = 1.732\,596$ and $L = 524\,140$. For the upper curve (scheme A) each run started from a periodic configuration, while the lower curve (scheme B) used for each run the final state of the previous run, with half of the sites with $z_i = 2$ declared as unstable. Each curve is based on 508 runs. The inset shows the same data multiplied by $t^{1/8}$. They coincide for $t > 10^4$ within statistical errors. The straight lines in the inset indicate the error ± 0.002 of θ.

Thus, simulations of single avalanches where the evolution is stopped at finite times seem not very useful. But, simulations near criticality where a finite fraction (50%, say) of sites with $z_i = 2$ are initially unstable are useful, and are crucial for understanding scaling. Let us denote by $\epsilon = \langle z\rangle - z_c$ the distance from the critical point. Naively, one should expect that activity satisfies in this case a finite-size scaling (FSS) ansatz

$$\rho_a(t,L,\epsilon) \sim t^{-\theta} F(\epsilon L^{1/\nu}, \epsilon t^{1/\nu_t}) \tag{29}$$

with $\nu_t = z\nu$. In order to agree with Eq. (18), the scaling function $F(x,y)$ has to scale for $y \to 0$ and $x \to \infty$ as y^β and furthermore $\theta = \beta/\nu_t$. The problem is of course that we expect this to hold when the state at $t = 0$ is a NCS, but we have no foolproof way to construct one. Even worse, a NCS would have no unstable sites. In studying single avalanches, it seems reasonable that declaring a single $z_i = 2$ site as unstable should be a negligible perturbation, but now we want to make a finite fraction unstable. It is far from obvious what effect this has, but we can turn to simulations to find out numerically.

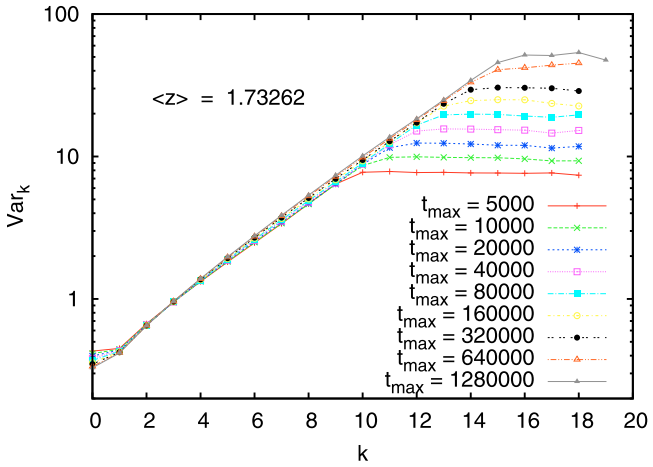

FIG. 19. Log-log plot of variances of the total stress on intervals of length 2^k, $\mathrm{Var}_k = \mathrm{Var}[Z_k]$ with $Z_k = \sum_{i=i_0}^{i_0+k-1 \bmod L} z_i$. Each curve was obtained by terminating the evolution of avalanches at t_{max}, and the total CPU time used for each curve was roughly the same. Lattice sizes were up to 4×10^6, and $\langle z\rangle$ is very close to critical.

Assume we want to use Eq. (29) to estimate θ from simulations up to time t_{max}, and let us assume that declaring half of the stable $z_i = 2$ sites as unstable does not create any problem (we shall come back to this later). If we rule out the option that we make first auxiliary runs up to $t \gg t_{max}$ in order to be sure that we have critical correlations up to and beyond the needed length scale, two options are left:

(i) We start each run from an uncorrelated periodic configuration, hoping that correlations build up sufficiently rapidly so that at late times the evolution proceeds effectively in a NCS (scheme A);

(ii) We keep the configuration of the previous run and declare half of the $z_i = 2$ sites as unstable (scheme B).

If both schemes lead to the same results, it is reasonable to assume that the results are reliable.

Results obtained with these two schemes are shown in Fig. 20. There, we used a large enough lattice ($L \approx 2^{15}$) and $\langle z\rangle$ sufficiently close to z_c that we expect a pure power law for large t. Both schemes lead indeed to the same power law

$$\rho_a(t) \sim t^{-\theta}\ , \quad \theta = 1/8 \pm 0.002. \tag{30}$$

On the other hand, both schemes show corrections for intermediate t. For scheme A they seem to be a simple power law, but for B they are more complicated: there is a depletion for $10 < t < 10^3$ which indicates that declaring half of the $z_i = 2$ sites in the NCS as unstable is indeed a too violent perturbation. This is even more pronounced for supercritical simulations, where scheme B gives very deep minima for intermediate t (see Fig. 21). We thus conclude that scheme

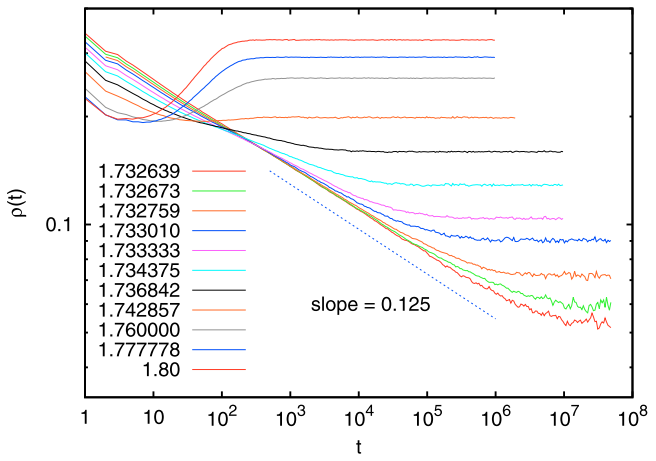

FIG. 21. Activity densities for supercritical FES systems, large enough to have negligible finite-size effects. Initial configurations were chosen according to scheme A. The numbers in the legend indicate $\langle z\rangle$ (top curve has largest $\langle z\rangle$).

A gives, in spite of showing substantial finite-t corrections, more reliable results that are easier to interpret. Final results are shown in Fig. 22. Figure 22(a) shows $\rho_a(t)$ against t for a few selected near critical values of $\langle z\rangle$, while Fig. 22(b) shows a collapse plot for the entire set of data in a rather wide range of $\langle z\rangle$. The structure near the the origin is due to the finite-time corrections mentioned above. Apart from that we see a perfect data collapse, indicating that indeed $\theta = \frac{1}{8}$ and

$$\nu_t = 40/21. \tag{31}$$

Notice that Eq. (28) can now be written as

$$\delta + \eta + \theta = 1/z \tag{32}$$

in which form it is just the generalized hyperscaling relation for systems with multiple absorbing states proposed in [56]. Defining $\beta' = \nu_t \delta$ as in [56], this gives

$$\beta' = 1/3 \neq \beta, \tag{33}$$

showing again that the model is not in the DP universality class, where $\beta' = \beta$.

E. Bulk-driven open systems

As we discussed in Sec. III A, the statistical properties of the stationary state are identical to those for boundary driving, thus we only have to discuss here the properties of avalanches. We again expect the scaling law (9) to hold, with the same exponent D. But, τ should now be different [39] because now $\langle s\rangle \sim L^2$. Assuming Eq. (9) we obtain

$$\tau_{\text{bulk}} = 2 - 2/D = 10/9. \tag{34}$$

This should hold for any open system with large L, where stress is added at sites far from the boundaries. We shall discuss later the case where stress is added only at the center region, but let us first discuss the case of uniform driving which was considered, e.g., in [39,57].

In this case, the stress is not always added at sites far from the boundary, and corrections to scaling could be large, but the scaling could hold nevertheless. To test this, we plotted in

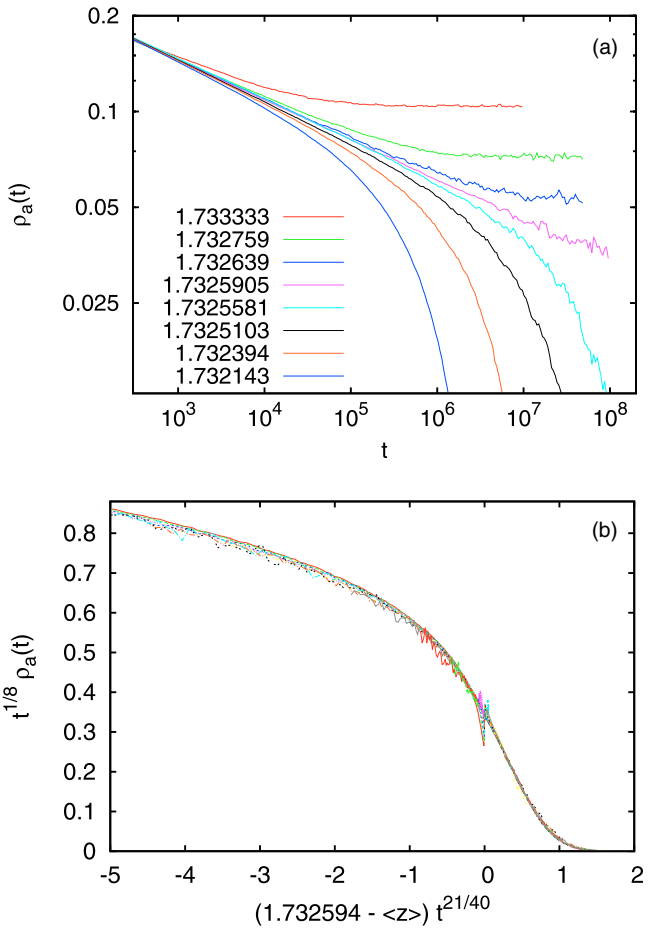

FIG. 22. (a) Activity densities for near critical FES systems. Initial conditions used scheme A, and lattices are large enough to have negligible finite-size effects. The numbers in the legend indicate $\langle z\rangle$ (top curve has largest $\langle z\rangle$). (b) Data collapse obtained by plotting $t^{1/8}\rho_a(t)$ against $(z_c - \langle z\rangle)t^{1/\nu_t}$ with $\nu_t = 40/21$. There are altogether 27 curves overlaid in this plot, for $\langle z\rangle$ ranging from 1.7143 to 1.7391.

Fig. 23(a) $s^{10/9}P(s,L)$ against $s/L^{9/4}$. If scaling were perfect, this would lead to a perfect data collapse. This is obviously not true (thus the fact that some avalanches start near a boundary is not negligible), but it seems to become true in the limit $L \to \infty$. In any case, both the position and the height of the peak scale in the right way. This means that avalanches starting near the boundaries do not contribute to the peak, as we should expect.

More interesting is the case of center driving because there we expect cleaner scaling than in case of uniform driving, although not as clean as for boundary driving. This is indeed seen in Fig. 23(b), but the improvement over uniform driving is rather modest.

Both for center driving and for uniform driving we also measured moments of T. Ratios $\langle T^k\rangle/\langle T^{k-1}\rangle$ showed now clean power laws for both $k = 2$ and 3, with exponent $z = 1.426(5)$, consistent with the previous estimate. But, in contrast to boundary driving, also $\langle T\rangle$ showed a power law with exponent 1.19(1).

Finally, we show in Fig. 24 results for the temporal evolution of avalanches similar to those shown in Fig. 11

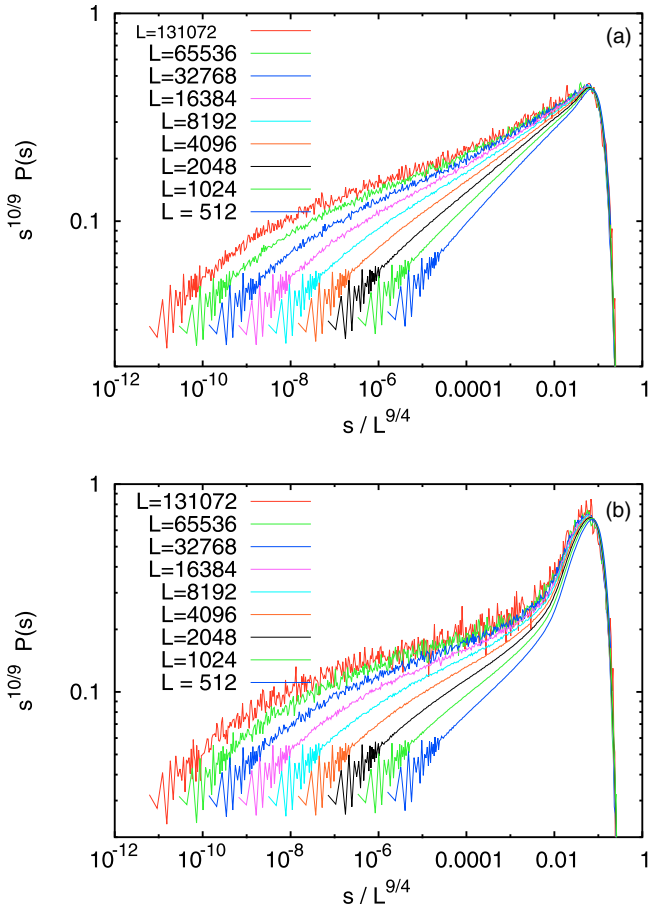

FIG. 23. Log-log plot of $s^{10/9}P(s,L)$ against $s/L^{9/4}$ for bulk-driven open systems. In (a) the driving is uniformly distributed over the entire region $[1,L]$, while in (b) the center sites are driven. In both cases, we see huge violations of scaling, which are biggest for uniform driving.

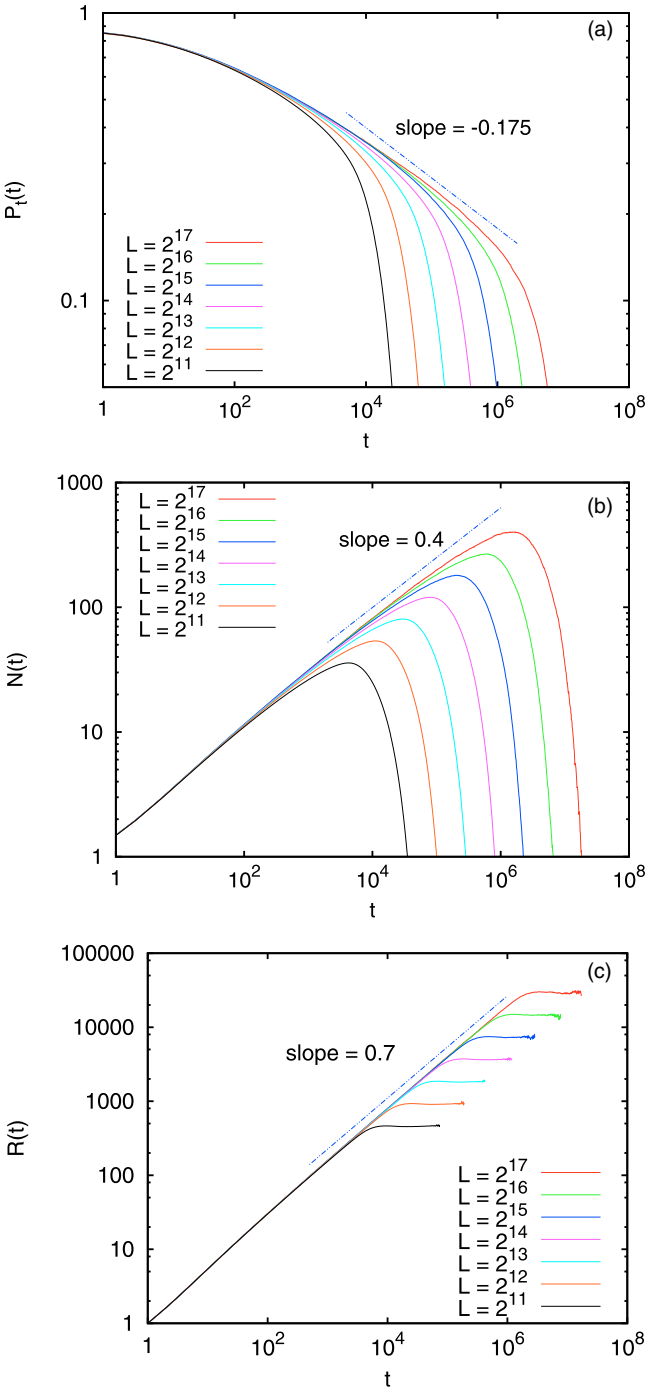

FIG. 24. Log-log plot of $P_t(t,L)$ (a), $N(t,L)$ (b), and $R(t,L)$ (c) for center-driven systems, similar to Fig. 11 for boundary-driven avalanches. The straight lines indicate power laws in the central (scaling) region.

for the boundary-driven case. Again, these data show much poorer scaling. The only curve that shows a convincing power law is that for $R(t)$ (which is now defined as the root mean square distance), and which clearly shows the same value for the dynamical exponent z. The exponents δ and η are clearly different from those for boundary-driven systems. In view of the large deviations from scaling, the estimates

$$\delta_{\rm bulk} = 7/40\,, \quad \eta_{\rm bulk} = 2/5 \tag{35}$$

seem not very well justified by the data alone, but they are consistent with the fixed-energy results presented in the last subsection.

IV. MAPPING ONTO AN INTERFACE MODEL

Following [38], we define an interface without overhangs by identifying its height $H(i,t)$ with the number of topplings up to (and including) time t. Alternatively [58], we could define another interface with height $h(i,t)$ such that $h(i,t)$ is the number of stress units *received* by topplings from its neighboring sites. The two heights are related by [58]

$$h(i,t) = H(i-1,t) + H(i+1,t). \tag{36}$$

On the other hand, the evolution of z_i can be written as

$$\begin{aligned} z_{i,t} - z_{i,0} &= h(i,t) - 2H(i,t) \\ &= H(i-1,t) + H(i+1,t) - 2H(i,t) \\ &\equiv \partial_i^2 H(i,t), \end{aligned} \tag{37}$$

where ∂_i^2 is the discrete Laplacian. Finally, the number of topplings at (i,t) is just a (random) function of $z_{i,t}$,

$$H(i,t+1) - H(i,t) = \sigma(z_{i,t}) \tag{38}$$

with

$$\sigma(z) = \begin{cases} 0 & \text{if } z \leqslant 1, \\ 1 & \text{if } z > 2, \\ 0 \text{ or } 1 & \text{with probability } 1/2, \text{ if } z = 2. \end{cases} \tag{39}$$

The last equations can be summarized as

$$\partial_t H(i,t) = \partial_i^2 H(i,t) + \eta(z_{i,t}, z_{i,0}) \tag{40}$$

with $\eta(x,y) = \sigma(x) - x + y$. This looks formally like the qEW equation [59]

$$\partial_t H(i,t) = \partial_i^2 H(i,t) + \eta[i; H(i,t)] \tag{41}$$

except that in the latter the noise η depends only on i and $H(i,t)$. In Eq. (40), in contrast, there is explicit dependence on the stresses $z_{i,t}$. Note that in Eq. (40), unlike the qEW equation, the noise depends not only on a quenched variable at the site in question, but also on the curvature of the interface.

Thus, the Oslo model is not exactly equivalent to the standard qEW model based on the interface H, where the noise correlations are

$$\langle \eta(t,H)\eta(t',H')\rangle = \delta_{t,t'}\delta_{H,H'}. \tag{42}$$

Because h is an explicit function of H due to Eq. (36), this is also true if H is exchanged by h, in contrast to what is claimed in [58]. It is also not true that H and h have different scaling properties, as was claimed in [58,60]. As should be clear from Eq. (36), and as will be verified numerically, they show exactly the same scaling.

Let us finally discuss the interface interpretation of the original Oslo model which is driven from its left border. As shown in [38], this corresponds to an interface that is prevented from being pinned by pulling slowly up the leftmost point. Consider the case where the interface is at its left end pulled by an amount $H(1,t) \gg L$, after which the pulling stops. In this case, the left hand side of Eq. (41) vanishes, and it can be written as

$$H(i+1,t) = 2H(i,t) + \eta[i,H(i,t)] - H(i-1,t), \tag{43}$$

showing that the evolution in the variable i, considered as a "time" evolution, is Markovian. Moreover, since the noise is assumed to be zero in average, the averaged heights satisfy simply $\partial_i^2\langle H(i,t)\rangle = 0$, showing that the average height profile is just linear.

We have already discussed the main idea of the mapping on the qEW model, and we have already given the numerical value of the exponent, called usually θ in the qEW model, that describes how the average interface velocity increases with the distance from the critical point. Here, we shall discuss more relations of this type. An annoying problem in doing so is the fact that equivalent exponents are given different names in the Oslo and qEW interpretations. We shall deal with it by adding a subscript "qEW" to all qEW exponents, e.g., $v \sim (F - F_c)^{\theta_{\rm qEW}}$ (notice that z and v are defined in the same way in the Oslo and qEW models). In the following, we shall discuss only the behavior exactly at the critical point, which we approximate to sufficient precision as $\langle z\rangle = 473/273 = 1.732\,601$. As we said in Sec. II, there are two slightly different mappings from the Oslo model onto the interface model. In the first, $h(i,t)$ is the number of stress units received at site i up to (and including) time t, while in the other $H(i,t)$ is the number of topplings.

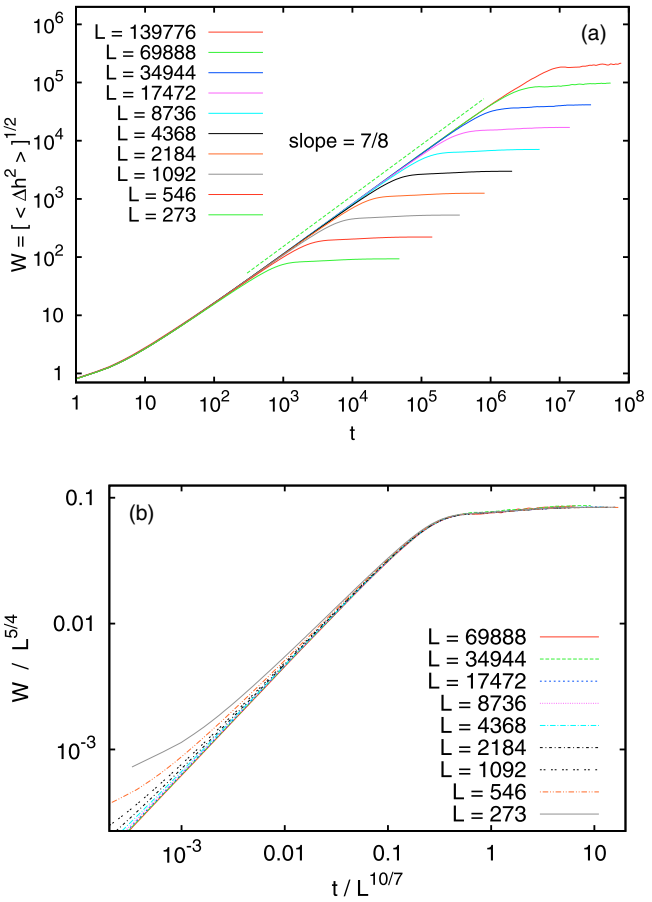

FIG. 25. Roughness W of interfaces constructed from the FES Oslo model, on lattices with density $\langle z\rangle = 473/273 = 1.732\,601$ and lattice sizes which are multiples of 273. (a) Shows the raw data, while (b) shows a data collapse obtained by plotting $L^{-\alpha_{\rm qEW}} W$ against t/L^z. In this and the following two figures, averages are taken over all runs, those which are still active at time t and those which had already died. If we had excluded the latter from the averages, interfaces would be slightly less rough (roughness increases sharply immediately before interfaces get pinned), but this would not affect their scaling (while it would affect the scaling of *average* height).

Let us first discuss how the global roughness of an interface h of base L increases at the critical force with time. The roughness is defined as the square root of $W^2 = \langle[\Delta h(t)]^2\rangle$, where angular brackets stand for an ensemble average and

$$[\Delta h(t)]^2 = \frac{1}{L}\sum_i h(i,t)^2 - \left[\frac{1}{L}\sum_i h(i,t)\right]^2. \tag{44}$$

Results are shown in Fig. 25. They demonstrate the well known behavior

$$W(t,L) = t^{\beta_{\rm qEW}} f(t/L^z) = L^{\alpha_{\rm qEW}} \tilde{f}(t/L^z) \tag{45}$$

with $\beta_{\rm qEW} = 1 - \theta = \frac{7}{8}$ and $\alpha_{\rm qEW} = z\beta_{\rm qEW} = \frac{5}{4}$. The most precise previous estimates of the exponents were in [52,54]. They are, respectively, $\beta_{\rm qEW} = 0.871(3)$ [0.872(3)], $\alpha_{\rm qEW} = 1.250(3)$ [1.250(3)], and $z = 1.440(15)$ [1.443(7)], and are somewhat less precise than our estimates.

Since $\alpha_{\rm qEW} > 1$ (critical qEW interfaces are "superrough"), the local slope of a critical interface cannot be bounded [61], and local roughnesses (i.e., roughnesses measured on a length scale $d \ll L$) must still increase for times at which an interface of total length d would already be pinned. Thus, the roughness of a part of length d of an interface of base $L \gg d$ satisfies "anomalous scaling" [62]

$$W(d;t,L) \sim \begin{cases} t^{\beta_{\rm qEW}} & \text{for } t \ll d^z, \\ d^{\alpha_{\rm loc}} L^{\alpha_{\rm qEW}-\alpha_{\rm loc}} & \text{for } d \ll L \ll t^{1/z}, \\ d^{\alpha_{\rm loc}} t^{(\alpha_{\rm qEW}-\alpha_{\rm loc})/z} & \text{for } d \ll t^{1/z} \ll L, \end{cases} \quad (46)$$

where $\alpha_{\rm loc}$ is a new exponent which for consistency must be $\leqslant 1$. In [62], $\alpha_{\rm qEW} - \alpha_{\rm loc}$ was called $\kappa/2$, but we shall follow [60,63] and define

$$\kappa = \frac{\alpha_{\rm qEW} - \alpha_{\rm loc}}{z}, \quad (47)$$

so that the scaling for intermediate times reads as now

$$W \sim d^{\alpha_{\rm loc}} t^{\kappa} \quad \text{for } d \ll t^{1/z} \ll L. \quad (48)$$

If the Oslo model is in the qEW universality class, the interfaces it is mapped onto must also satisfy these scaling relations. In order to test this, we show local roughnesses of $h(i,t)$ in Figs. 26(a) and 26(b), while local roughnesses of $H(i,t)$ are shown in Fig. 26(c). All three panels in Fig. 26 show data for $L = 131\,040$ and $\langle z\rangle = 473/273$. Figure 26(a) shows a log-log plot of the square of the roughness against t. Each curve corresponds to a distance $d = 2^k$, $k = 1,3,5,\ldots,15$ over which the roughness is computed. It is defined as $W^2(d;t,L) = \langle [h(i,t) - h(i+d,t)]^2\rangle$. We see clearly the two scaling laws $W(d;t,L) \sim t^{\beta_{\rm qEW}}$ for $t < d^z$ with $\beta_{\rm qEW} = 0.875$, and Eq. (48) with $\kappa = 7/40 \pm 0.01$. Notice that the latter holds for all d, even for $d = 1$ (not shown). Figure 26(b) shows the same data, but in order to see more clearly the value of $\alpha_{\rm loc}$ we divided the roughness by d. We see a perfect data collapse for $t \gg 1$ and $d \ll t^{1/z}$, which implies that

$$\alpha_{\rm loc} = 1, \quad (49)$$

in agreement with our estimate $\kappa = \frac{7}{40}$. Finally, Fig. 26(c) is completely analogous to Fig. 26(a), except that it shows roughnesses of the interface $H(i,t)$ which is obtained from the number of topplings instead of the number of units received by a site. It clearly demonstrates that both interface definitions lead to the same scaling.

Our result $\alpha_{\rm loc} = 1$ is obtained in many different 1D interface models [62,63], but to our knowledge it cannot be derived analytically for the qEW model. Previous numerical estimates [64] agree with it. On the other hand, our finding that the interfaces $H(i,t)$ and $h(i,t)$ satisfy the same scaling disagrees with claims made in [58,60]. In particular, we find for both the same exponent κ. This value agrees with what is called "A scaling" in [60]. In contrast to claims made in [60], the Oslo model seems incompatible with what is called there "B scaling." For a possible explanation of that contradiction, see [66].

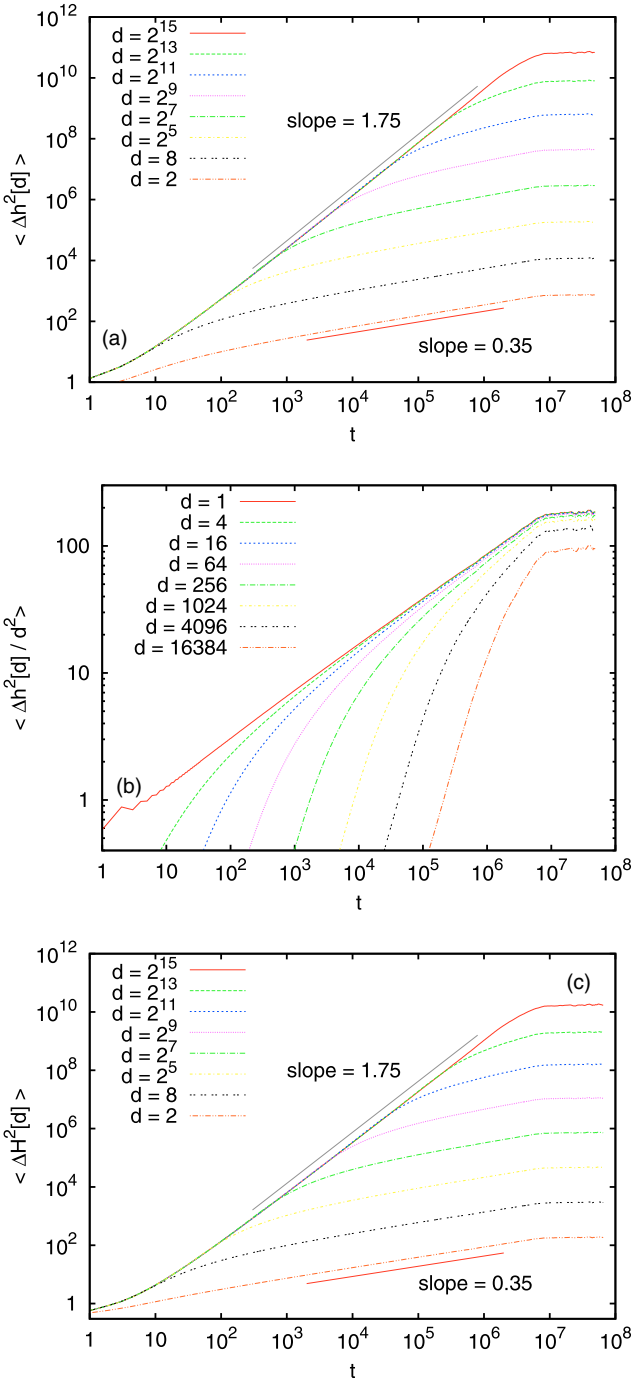

FIG. 26. (a) Log-log plot of local squared roughnesses of interfaces constructed from the FES Oslo model, on lattices with density $\langle z\rangle = 473/273 = 1.732\,601$ and size $L = 131\,040$. The straight lines indicate the anomalous roughening power laws. (b) Shows the same data, but divided by d^2. According Eq. (46) one should see a data collapse for $d \ll t^{1/z} \ll L$. There is indeed a perfect collapse for $t \approx 10^6$, if the largest distances d are discarded. Panel (c), finally, is analogous to (a) but shows data for the alternative interface definition that is based on number of *topplings* instead of *received* units of stress.

V. CONCLUSIONS

Part of the motivation for this work was the observation that natural critical state in the Oslo model is models are hyperuniform. On the one hand, this suggests that transients in simulations could be cut short by starting from very uniform initial configurations. This was indeed found, and it allowed the simulation of much bigger systems than previously possible.

On the other hand, it suggested that, if the hyperuniformity is strong enough, the conserved field in sand-pile models can be considered as rigid and nonfluctuating, in which case these models would be in the same universality class as directed percolation. We find that this is not so (see also [28]). Instead, we find compelling evidence that the one-dimensional Oslo model is in the same universality class as the qEW (or linear interface) model. This had been a long-standing conjecture, but it had been repeatedly doubted due to contradictory numerical results. One main reason for these numerical problems was precisely that hyperuniformity had not been taken into account. In a forthcoming paper [67], we will discuss some other Oslo-type models with directed particle transfer rules on two-dimensional lattices, which turn out to correspond to an Edwards-Wilkinson interface model *with annealed noise*.

An unexpected outcome of this work is that the vastly improved simulations (made possible in part by judicious choices of initial conditions) suggest that the critical exponents of the 1D Oslo model (and, more importantly, also the 1D qEW model) are simple rational numbers. For some exponents, this had already been conjectured before, but not (to our knowledge) for the dynamical and hyperuniformity exponents, and for the exponent σ [see Eq. (5)] describing the stress profile in the case of open boundaries. Also, these exponents fall outside the infinite series of discrete rational exponents recently found for 1D stochastic models [68]. Of course, in the same study, well-behaved models where the dynamical exponent is the golden mean, i.e., an irrational value have also been discussed. So, while the critical exponents do not *have to be* rational, we note that most soluble models so far have found rational critical exponents. Showing that these conjectured values are actually correct remains a challenge.

Our finding that the 1D Oslo model is in the qEW universality class suggests of course that the same could be true for other stochastic sand-pile models, and for SOC models with conserved fields in higher dimensions. This does not invalidate our earlier argument about instability of the Manna model fixed point under suitable perturbation to DP. All this says is that adding this kind of perturbation (say adding a small probability of z_c being set to 3, $z_c = 2$ is the deterministic sand pile) does not constitute such a relevant perturbation.

In fact, we have to conclude that there is no single unique universality class for stochastic sand-pile models. One has different critical behaviors, depending on the details of the model. For example, if in the toppling process we add randomness also in where the transferred particles may go (as in the original Manna model), then the critical behavior of the model would change. In fact, other stochastic 1D sand-pile models (like the Maslov-Zhang model [13] or the continuous Manna model [17]) appear to have critical exponents different from the Oslo model studied here. Thus, there is no unique fixed point corresponding to a "generic behavior." Further studies are needed to identify all the different possible behaviors.

ACKNOWLEDGMENTS

P.G. thanks the Leverhulme trust for financial support, and the University of Aberdeen, where part of this work was done, for a most pleasant stay. D.D.'s research is supported partially by the Indian Department of Science and Technology via Grant No. DST-SR/S2/JCB-24/2005.

[1] P. Bak, C. Tang, and K. Wiesenfeld, Phys. Rev. Lett. **59**, 381 (1987).
[2] E. V. Ivashkievich, D. V. Ktitarev, and V. B. Priezzhev, Phys. A (Amsterdam) **209**, 347 (1994).
[3] D. V. Ktitarev, S. Lübeck, P. Grassberger, and V. B. Priezzhev, Phys. Rev. E **61**, 81 (2000).
[4] D. Dhar, Phys. A (Amsterdam) **369**, 29 (2006).
[5] F. Redig, *Les Houches*, Vol. 83, edited by A. Bovier *et al.* (Elsevier B.V., 2006), pp. 657–659, pp. 661–729.
[6] L. Levine and J. Propp, Notices AMS **57**, 976 (2010).
[7] C. Tebaldi, M. De Menech, and A. L. Stella, Phys. Rev. Lett. **83**, 3952 (1999).
[8] A. Ben-Hur and O. Biham, Phys. Rev. E **53**, R1317 (1996).
[9] O. Biham, E. Milshtein, and O. Malcai, Phys. Rev. E **63**, 061309 (2001).
[10] S. S. Manna, J. Phys. A: Math. Gen. **24**, L363 (1991).
[11] V. Frette, K. Christensen, A. Malthe-Sørensen, J. Feder, T. Jøssang, and P. Meakin, Nature (London) **379**, 49 (1996).
[12] Y.-C. Zhang, Phys. Rev. Lett. **63**, 470 (1989).
[13] S. Maslov and Y.-C. Zhang, Phys. A (Amsterdam) **223**, 1 (1996).
[14] M. Rossi, R. Pastor-Satorras, and A. Vespignani, Phys. Rev. Lett. **85**, 1803 (2000).
[15] P. K. Mohanty and D. Dhar, Phys. Rev. Lett. **89**, 104303 (2002).
[16] P. K. Mohanty and D. Dhar, Phys. A (Amsterdam) **384**, 34 (2007).
[17] M. Basu, U. Basu, S. Bondyopadhyay, P. K. Mohanty, and H. Hinrichsen, Phys. Rev. Lett. **109**, 015702 (2012).
[18] C. Tang and P. Bak, Phys. Rev. Lett. **60**, 2347 (1988).
[19] C. Tang and P. Bak, J. Stat. Phys. **51**, 797 (1988).
[20] P. Grassberger and S. S. Manna, J. Phys. **51**, 1077 (1990).
[21] H. Hinrichsen, Adv. Phys. **49**, 815 (2000).
[22] In the "random subtraction" version of the fixed-energy BTW model in [69], e.g., simulations were done at slightly subcritical densities (so that avalanches died), and new avalanches were triggered by moving one of the sand grains to a random arbitrarily far away site. It is not clear that the steady state produced this way is the same as what would be produced if the grain was moved only to nearest-neighbor site.
[23] V. Frette, Phys. Rev. Lett. **70**, 2762 (1993).
[24] K. Christensen, A. Corral, V. Frette, J. Feder, and T. Jossang, Phys. Rev. Lett. **77**, 107 (1996).

[25] D. Dhar, Phys. A (Amsterdam) **340**, 535 (2004).
[26] D. Hexner and D. Levine, Phys. Rev. Lett. **114**, 110602 (2015).
[27] S. B. Lee, Phys. Rev. E **89**, 060101 (2014).
[28] R. Dickman and S. D. da Cunha, Phys. Rev. E **92**, 020104(R) (2015).
[29] S. Torquato and F. H. Stillinger, Phys. Rev. E **68**, 041113 (2003).
[30] A. Gabrielli, M. Joyce, and F. S. Labini, Phys. Rev. D **65**, 083523 (2002).
[31] A. Fey, L. Levine, and D. B. Wilson, Phys. Rev. E **82**, 031121 (2010).
[32] The latter are the most "natural" b.c.'s if we concentrate on the z_i. Although a different b.c. at the right boundary was used in [11], we call Eq. (2) "the original Oslo model" since the difference is irrelevant for scaling.
[33] See Eq. (32) in [25].
[34] K. Christensen, N. R. Moloney, O. Peters, and G. Pruessner, Phys. Rev. E **70**, 067101 (2004).
[35] A. Vespignani, R. Dickman, M. A. Muñoz, and S. Zapperi, Phys. Rev. E **62**, 4564 (2000).
[36] A. Chua and K. Christensen, arXiv:cond-mat/0203260.
[37] G. Pruessner and H. J. Jensen, Phys. Rev. Lett. **91**, 244303 (2003).
[38] M. Paczuski and S. Boettcher, Phys. Rev. Lett. **77**, 111 (1996).
[39] K. Christensen, Phys. A (Amsterdam) **340**, 527 (2004).
[40] J. A. Bonachela, Universality in Self-Organized Criticality, Ph.D. thesis, University of Granada, 2008.
[41] R. Dickman, M. Alava, M. A. Munoz, J. Peltola, A. Vespignani, and S. Zapperi, Phys. Rev. E **64**, 056104 (2001).
[42] R. Dickman, T. Tome, and M. J. de Oliveira, Phys. Rev. E **66**, 016111 (2002).
[43] R. Dickman, Phys. Rev. E **66**, 036122 (2002).
[44] R. Dickman, Phys. Rev. E **73**, 036131 (2006).
[45] J. Kockelkoren and H. Chaté, arXiv:cond-mat/0306039.
[46] J. J. Ramasco, M. A. Munoz, and C. A. daSilva Santos, Phys. Rev. E **69**, 045105(R) (2004).
[47] S. Lübeck, Int. J. Mod. Phys. B **18**, 3977 (2004).
[48] E. Fiore and M. J. de Oliveira, Braz. J. Phys. **36**, 218 (2006).
[49] H. Leschhorn, Phys. A (Amsterdam) **195**, 324 (1993).
[50] O. Duemmer and W. Krauth, Phys. Rev. E **71**, 061601 (2005).
[51] J. M. Kim and H. Choi, J. Korean Phys. Soc. **48**, S241 (2006).
[52] H. S. Song and J. M. Kim, J. Korean Phys. Soc. **53**, 1802 (2008).
[53] A. Corral and M. Paczuski, Phys. Rev. Lett. **83**, 572 (1999).
[54] E. E. Ferrero, S. Bustingorry, and A. B. Kolton, Phys. Rev. E **87**, 032122 (2013).
[55] S. B. Lee, J. Korean Phys. Soc. **55**, 2339 (2009); **60**, 559 (2012).
[56] J. F. F. Mendes, R. Dickman, M. Henkel, and M. Ceu Marques, J. Phys. A: Math. Gen. **27**, 3019 (1994).
[57] A. Malthe-Sørensen, Phys. Rev. E **59**, 4169 (1999).
[58] G. Pruessner, Phys. Rev. E **67**, 030301 (2003).
[59] T. Nattermann, S. Stepanow, L.-H. Tang, and H. Leschhorn, J. Phys. II (France) **2**, 1483 (1992).
[60] J. A. Bonachela, H. Chaté, I. Dornic, and M. A. Muñoz, Phys. Rev. Lett. **98**, 155702 (2007).
[61] H. Leschhorn and L.-H. Tang, Phys. Rev. Lett. **70**, 2973 (1993).
[62] S. Das Sarma, S. V. Ghaisas, and J. M. Kim, Phys. Rev. E **49**, 122 (1994).
[63] J. M. López, Phys. Rev. Lett. **83**, 4594 (1999).
[64] J. M. López and M. A. Rodriguez, J. Phys. I (France) **7**, 1191 (1997).
[65] J. A. Bonachela, Universality in self-organized criticality, Ph.D. Thesis, University of Granada, 2008.
[66] Our claim agrees indeed with the thesis of Bonachela [65], where it is correctly said on p. 142 that B scaling is expected for the Manna model, but not for Oslo. More precisely, in the Manna model h and H should show different local roughnesses because there Eq. (36) contains additional noise terms resulting from the randomness of the toppling. These noise terms are absent in the Oslo model. As a consequence, h is locally more rough than H in case of the Manna model (and in other models with random topplings), but not in case of the Oslo model. This suggests that including the Oslo model in [60] in the list of models with both A and B scaling was just a glitch.
[67] P. K. Mohanty, D. Dhar, and P. Grassberger (unpublished).
[68] V. Popkov, A. Schadschneider, J. Schmidt, and G. M. Schütz, Proc. Natl. Acad. Sci. U.S.A. **112**, 12645 (2015).
[69] A. Chessa, E. Marinari, and A. Vespignani, Phys. Rev. Lett. **80**, 4217 (1998).